RESEARCH ARTICLE | DECEMBER 16 2025

Reversed Cherenkov radiation via Fizeau–Fresnel drag

Bowen Zhang ; Zheng Gong ; Ruoxi Chen ; Xuhuinan Chen ; Yi Yang ; Hongsheng Chen ; Ido Kaminer ; Xiao Lin

Appl. Phys. Rev. 12, 041421 (2025)
https://doi.org/10.1063/5.0296513

Applied Physics Reviews ARTICLE pubs.aip.org/aip/are

Reversed Cherenkov radiation via Fizeau–Fresnel drag

Cite as: Appl. Phys. Rev. **12**, 041421 (2025); doi: 10.1063/5.0296513
Submitted: 13 August 2025 · Accepted: 4 December 2025 ·
Published Online: 16 December 2025

View Online Export Citation CrossMark

Bowen Zhang,[1,2] Zheng Gong,[1,2] Ruoxi Chen,[1,2] Xuhuinan Chen,[1,2] Yi Yang,[3] Hongsheng Chen,[1,2,a)] Ido Kaminer,[4,a)] and Xiao Lin[1,2,a)]

AFFILIATIONS

[1]State Key Laboratory of Extreme Photonics and Instrumentation, Zhejiang Key Laboratory of Intelligent Electromagnetic Control and Advanced Electronic Integration, Interdisciplinary Center for Quantum Information, College of Information Science & Electronic Engineering, Zhejiang University, Hangzhou 310027, China
[2]International Joint Innovation Center, The Electromagnetics Academy at Zhejiang University, Zhejiang University, Haining 314400, China
[3]Department of Physics, HK Institute of Quantum Science and Technology, University of Hong Kong, Hong Kong 999077, China
[4]Department of Electrical and Computer Engineering, Technion-Israel Institute of Technology, Haifa 32000, Israel

[a)]Author to whom correspondence should be addressed: hansomchen@zju.edu.cn; kaminer@technion.ac.il; and xiaolinzju@zju.edu.cn

ABSTRACT

It has long been thought that the reversed Cherenkov radiation is impossible in homogeneous media with a positive refractive index n. Here, we break this long-held belief by revealing the possibility of creating reversed Cherenkov radiation from homogeneous positive-index moving media. The underlying mechanism is essentially related to the Fizeau–Fresnel drag effect, which provides a unique route to drag the emitted light in the direction of the moving medium and thus enables the possibility of dragging the emitted light in the opposite direction of the moving charged particle. Moreover, we discover the existence of a threshold for the velocity v_{medium} of moving media, only above which, namely, $v_{\text{medium}} > c/n^2$, the reversed Cherenkov radiation may emerge, where c is the velocity of light in vacuum. Particularly, we find that the reversed Cherenkov radiation inside superluminal moving media (i.e., $v_{\text{medium}} > c/n$) can become thresholdless for the velocity of moving charged particles.

Relativistic motion is widely known to have peculiar effects across all domains of physics,[1–9] especially on the electromagnetic interactions of charged particles. One paradigmatic phenomenon is the Cherenkov radiation,[10–16] which is essentially induced by the relative motion between charged particles and the surrounding medium with a refractive index n. Specifically, Cherenkov radiation emerges when a charged particle moves with a velocity v_e exceeding the so-called Cherenkov threshold, namely, the phase velocity c/n of light in the surrounding stationary medium, where c is the velocity of light in vacuum. One powerful implication of Cherenkov radiation is its directionality across a broad spectral regime, ranging from microwave to terahertz, infrared, visible, ultraviolet, and X-ray.[17–19] Accordingly, Cherenkov radiation is of paramount importance to enormous practical applications,[20–23] including particle detectors for the identification of high-energy particles,[24–29] light sources at previously hard-to-reach frequencies,[30–33] bio-medical imaging,[34–36] and photodynamic therapy.[37–39]

Soon after the experimental discovery of Cherenkov radiation by Cherenkov under the guidance of Vavilov in 1934,[40] their finding was successfully interpreted by Frank and Tamm in 1937 based on the classic electrodynamic theory.[41] According to the well-known Frank–Tamm formula $\cos\theta = c/nv_e$ for stationary media,[42] the Cherenkov radiation angle θ is uniquely related to the particle velocity v_e. Moreover, the conventional Cherenkov radiation generally has $\theta < 90°$ in stationary positive-index media with $n > 0$. Under this scenario, the emitted light would propagate in the same direction as the emitting particle.

In contrast, the reversed Cherenkov radiation[43–46] has $\theta > 90°$, so that the emitted light would propagate in the reversed or opposite direction of particle motion. According to the pioneering prediction of Veselago in 1968,[43] the realization of reversed Cherenkov radiation requires novel materials, namely, materials with a negative refractive index. As a result, both theoretical prediction and experimental observation of reversed Cherenkov radiation are so far limited to the framework of unconventional homogeneous materials (e.g., negative-index materials[47–51] and anisotropic materials[52–56]) or judiciously designed inhomogeneous structures (e.g., gain slabs[57] and photonic crystals[58–60]). In fact, it is widely believed that the reversed Cherenkov radiation is impossible in homogeneous positive-index media. Here, we reveal a universal route to create the reversed Cherenkov radiation from homogeneous positive-index moving media. Our finding thus breaks this long-held tenet.

In general, the surrounding medium is not necessarily stationary but can be in motion. The moving media, such as the flowing water, are ubiquitous around us. This way, it is natural to ask whether the motion of positive-index media can provide an extra degree of freedom to enable the emergence of reversed Cherenkov radiation. Somehow, this open scientific question remains underexplored; particularly, whether the creation of reversed Cherenkov radiation has any fundamental restriction on the motion velocity of positive-index media remains elusive.

To address this issue, we find the possibility to create the reversed Cherenkov radiation from homogeneous positive-index moving media by exploiting the Fizeau–Fresnel drag effect. The underlying mechanism is that since the Fizeau–Fresnel drag effect is capable of dragging the emitted light toward the direction of moving media, the Fizeau–Fresnel drag effect provides the enticing possibility to drag the emitted light toward the reversed direction of moving charged particles. As background, the Fizeau–Fresnel drag effect[61–63] was first postulated by Fresnel in 1818,[64] experimentally verified by Fizeau in 1851[65] and later helped shape the theory of relativity[66,67] and facilitated the analysis of quantum friction.[68–71] Despite the long research history of free-electron radiation[72–81] and the Fizeau–Fresnel drag effect,[82–88] we highlight that the intrinsic connection between the reversed Cherenkov radiation and the Fizeau–Fresnel drag effect has never been explored before. Moreover, we discover that the reversed Cherenkov radiation may occur, only when the medium velocity $v_{\rm medium}$ exceeds a critical threshold c/n^2, namely, $v_{\rm medium} > c/n^2$. That is, the reversed Cherenkov radiation from positive-index moving media may emerge when the medium velocity is either subluminal (i.e., $c/n^2 < v_{\rm medium} < c/n$) or superluminal (i.e., $v_{\rm medium} > c/n$). Remarkably, under the superluminal scenario with $v_{\rm medium} > c/n$, we find the reversed Cherenkov radiation becomes intrinsically thresholdless for the velocity of moving charged particles.

Figure 1 shows the conceptual illustration of reversed Cherenkov radiation via Fizeau–Fresnel drag. The Fizeau–Fresnel drag effect can be vividly understood from the analysis of boat's motion on the flowing water in Figs. 1(a) and 1(b). Briefly speaking, while the boat moves toward the $-\hat{z}'$ direction under the water co-moving frame S' in Fig. 1(a), the boat may become to move toward the $+\hat{z}$ direction under the static river frame S in Fig. 1(b), due to the Fizeau–Fresnel drag

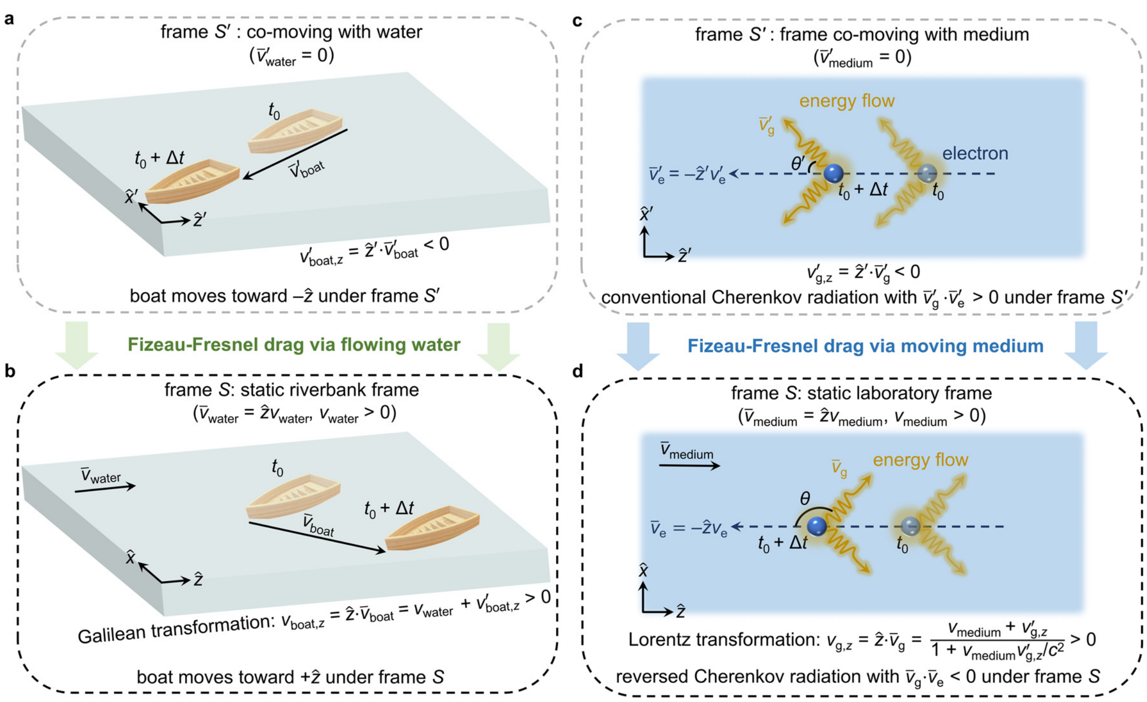

FIG. 1. Conceptual schematic of reversed Cherenkov radiation via Fizeau–Fresnel drag. (a) and (b) Fizeau–Fresnel drag of boat via flowing water. A boat moves with a velocity $\bar{v}'_{\rm boat}$ toward the $-\hat{z}'$ direction under the frame S' in (a), which is co-moving with water, namely, $v'_{\rm boat,\,z} = \hat{z}'\cdot\bar{v}'_{\rm boat} < 0$. Under the static riverbank frame S in (b), the water moves with a velocity $\bar{v}_{\rm water} = \hat{z}v_{\rm water}$ toward the $+\hat{z}$ direction, and the boat can move with a velocity $\bar{v}_{\rm boat}$ toward the $+\hat{z}$ direction if $v_{\rm boat,z} = \hat{z}\cdot\bar{v}_{\rm boat} = v_{\rm water} + v'_{\rm boat,z} > 0$ (i.e., $v_{\rm water} > |v'_{\rm boat,z}|$). (c) and (d) Fizeau–Fresnel drag of light via the moving medium. Under the frame S' co-moving with the medium in (c), an electron moves with a velocity $\bar{v}'_{\rm e} = -\hat{z}'v'_{\rm e}$, and the medium at rest has a positive refractive index n. Accordingly, the induced light emission has $\bar{v}'_{\rm g}\cdot\bar{v}'_{\rm e} > 0$ and corresponds to the conventional Cherenkov radiation, where $\bar{v}'_{\rm g}$ is the group velocity of light under the frame S'. Under the static laboratory frame S in (d), the medium moves with a velocity $\bar{v}_{\rm medium} = \hat{z}v_{\rm medium}$ toward the $+\hat{z}$ direction, and the electron has a velocity $\bar{v}_{\rm e} = -\hat{z}v_{\rm e}$. The light emission under the frame S can have $\bar{v}_{\rm g}\cdot\bar{v}_{\rm e} < 0$ and corresponds to the reversed Cherenkov radiation if $v_{\rm g,z} = \frac{v_{\rm medium}+v'_{\rm g,z}}{1+v_{\rm medium}v'_{\rm g,z}/c^2} > 0$ (i.e., $v_{\rm medium} > |v'_{\rm g,z}|$), where $v'_{\rm g,z} = \hat{z}'\cdot\bar{v}'_{\rm g}$ and $v_{\rm g,z} = \hat{z}\cdot\bar{v}_{\rm g}$.

applied by the flowing water on the boat. Similarly, the moving medium can act like the flowing water and apply the Fizeau–Fresnel drag on the propagating light emitted by charged particles (e.g., free electrons used below), as schematically shown in Figs. 1(c) and 1(d). Without loss of generality, below we assume that under the static laboratory frame S in Fig. 1(d), the medium moves toward the $+\hat{z}$ direction with a velocity $\bar{v}_{\rm medium} = \hat{z}v_{\rm medium}$ (i.e., $v_{\rm medium} > 0$), and the swift electron moves antiparallelly to the medium toward the $-\hat{z}$ direction with a velocity of $\bar{v}_{\rm e} = -\hat{z}v_{\rm e}$ (i.e., $v_{\rm e} > 0$).

We begin with the analysis under the medium co-moving frame S' in Fig. 1(c). For conceptual illustration, we set that the static isotropic medium is nondispersive, lossless and has a constant positive refractive index n ($n > 1$). According to the Lorentz transformation, the electron moves with a velocity of $\bar{v}'_{\rm e} = -\hat{z}'v'_{\rm e}$, where $v'_{\rm e} = \frac{v_{\rm e}+v_{\rm medium}}{1+v_{\rm e}v_{\rm medium}/c^2}$. Since $v_{\rm medium} > 0$ and $v_{\rm e} > 0$, we have $v'_{\rm e} > 0$. This way, under the frame S', the swift electron also moves toward the $-\hat{z}'$ direction. According to the Frank–Tamm formula, when $v'_{\rm e} > c/n$, the emitted light generally has $\bar{v}'_{\rm g} \cdot \bar{v}'_{\rm e} > 0$ and $\cos\theta' = c/nv'_{\rm e}$, where $|\bar{v}'_{\rm g}| = c/n$ is the group velocity of emitted light under the frame S' and θ' is the angle between $\bar{v}'_{\rm g}$ and $\bar{v}'_{\rm e}$ (or $-\hat{z}'$). Accordingly, we have $\theta' = \arccos(c/nv'_{\rm e}) < 90°$ and $v'_{{\rm g},z} = \hat{z}' \cdot \bar{v}'_{\rm g} = -|\bar{v}'_{\rm g}|\cos\theta' = -c/n \cdot c/nv'_{\rm e} = -c^2/n^2v'_{\rm e} < 0$, as schematically shown in Fig. 1(c). Since $v'_{{\rm g},z} < 0$, the emitted light should also propagate toward the $-\hat{z}'$ direction. This scenario essentially corresponds to the emergence of conventional Cherenkov radiation under the medium co-moving frame S' in Fig. 1(c).

We now proceed to the analysis under the static laboratory frame S in Fig. 1(d). According to the Lorentz transformation, the group velocity $\bar{v}_{\rm g}$ of emitted light under the frame S in Fig. 1(d) has

$$v_{{\rm g},z} = \hat{z} \cdot \bar{v}_{\rm g} = \frac{v_{\rm medium} + v'_{{\rm g},z}}{1 + v_{\rm medium}v'_{{\rm g},z}/c^2}. \tag{1}$$

Upon close inspection of $v_{{\rm g},z}$ in Eq. (1), its denominator is always positive, namely, $1 + v_{\rm medium}v'_{{\rm g},z}/c^2 > 0$, since $|v'_{{\rm g},z}| \le c$ and $v_{\rm medium} \le c$ according to the relativity theory.

To enable the emergence of reversed Cherenkov radiation with $\theta > 90°$ under the frame S, the emitted light should propagate to the reversed direction of electron's motion, namely, the $+\hat{z}$ direction, where θ is the angle between $\bar{v}_{\rm g}$ and $\bar{v}_{\rm e}$ (or $-\hat{z}$) under the frame S. In other words, $v_{{\rm g},z} > 0$ should be satisfied. Since the denominator of $v_{{\rm g},z}$ in Eq. (1) is positive, this actually requires the numerator of $v_{{\rm g},z}$ in Eq. (1) to be positive, namely,

$$v_{\rm medium} + v'_{{\rm g},z} = v_{\rm medium} - |v'_{{\rm g},z}| > 0. \tag{2}$$

Since $|v'_{{\rm g},z}| = c^2/n^2v'_{\rm e}$, Eq. (2) can be re-organized to

$$v_{\rm medium} > c^2/n^2v'_{\rm e} \quad \text{or} \quad v'_{\rm e} > c^2/n^2v_{\rm medium}. \tag{3}$$

Moreover, since $v'_{\rm e} \le c$, the necessary and sufficient condition to enable the emergence of reversed Cherenkov radiation can be obtained as

$$c \ge v'_{\rm e} > c^2/n^2v_{\rm medium}. \tag{4}$$

From Eq. (4), we must always have

$$v_{\rm medium} > c/n^2. \tag{5}$$

According to Eq. (5), the reversed Cherenkov radiation inside moving positive-index media may emerge only when the medium velocity $v_{\rm medium}$ exceeds the critical threshold $v_{\rm th,rCR,medium}$, namely, $v_{\rm medium} > v_{\rm th,rCR,medium}$, where

$$v_{\rm th,rCR,medium} = c/n^2. \tag{6}$$

The scaling factor $1/n^2$ could also be obtained via the geometric relation between the particle velocity and the group velocity of light, as shown in Fig. S5.

On the other hand, Eq. (5) indicates that the reversed Cherenkov radiation under the static laboratory frame S may emerge if the medium velocity is either superluminal ($v_{\rm medium} > c/n$) or subluminal ($c/n^2 < v_{\rm medium} < c/n$). For conceptual illustration, below $n = 2$ is used. To facilitate the understanding, the isofrequency contours of light inside the moving medium under the frame S, which are widely used in the analysis of quantum friction,[69] are plotted in Figs. 2 and 3. Specifically, these isofrequency contours of light inside the moving

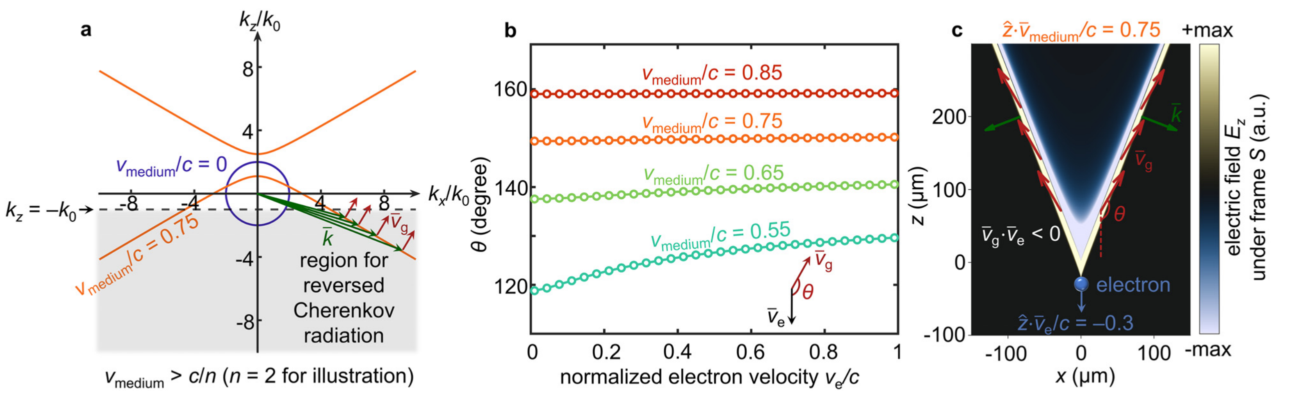

FIG. 2. Reversed Cherenkov radiation inside superluminal moving media. Here and below, we set the refractive index $n = 2$ for illustration. (a) Isofrequency contours of eigenmodes inside the moving medium. The dashed line corresponds to $k_z = -k_0$, where $k_0 = \omega/c$ is the wavevector of light in vacuum and ω is the angular frequency of emitted light. (b) Dependence of the radiation angle θ on the electron velocity $v_{\rm e}$ for various $v_{\rm medium}$, where θ is the angle between the group velocity $\bar{v}_{\rm g}$ of emitted light and $\bar{v}_{\rm e}$ (or $-\hat{z}$). (c) Distribution of the electric field E_z induced by the swift electron, where $v_{\rm medium}/c = 0.75$ and $v_{\rm e}/c = 0.3$.

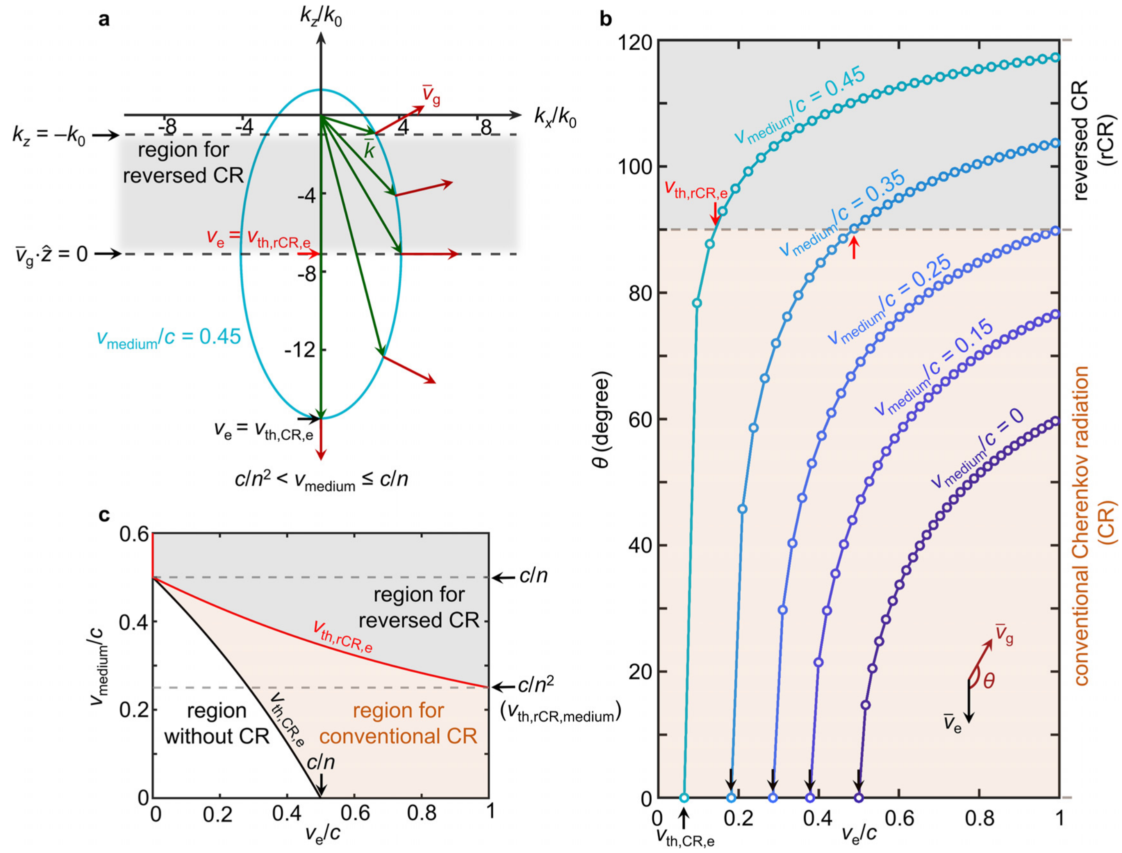

FIG. 3. Reversed Cherenkov radiation inside subluminal moving media. Under the laboratory frame S, $v_{th,CR,e}$($v_{th,rCR,e}$) corresponds to the threshold of electron velocity v_e for the conventional (reversed) Cherenkov radiation, and $v_{th,rCR,medium} = c/n^2$ corresponds to the threshold of medium velocity v_{medium} to enable the emergence of reversed Cherenkov radiation. (a) Isofrequency contour of eigenmodes of light inside the moving medium with $v_{meidum}/c = 0.45$. (b) Dependence of the radiation angle θ on the electron velocity v_e under various v_{medium}. (c) Phase diagram of Cherenkov radiation in the $v_e - v_{medium}$ parameter space.

medium under the laboratory frame S are governed by $k_x^2 + \frac{c^2-n^2v_{medium}^2}{c^2-v_{medium}^2}\left[k_z - \frac{nc+v_{medium}}{nv_{medium}+c}\frac{\omega}{c}\right]\cdot\left[k_z - \frac{nc-v_{medium}}{nv_{medium}-c}\frac{\omega}{c}\right] = 0$,[42] where ω and $\bar{k} = \hat{x}k_x + \hat{z}k_z$ are the angular frequency and the wavevector of light, respectively. From this equation, both the symmetry center and shape of the isofrequency contour essentially vary with the medium velocity v_{medium}. For example, distinct hyperbolic or elliptical isofrequency contours emerge in Figs. 2(a) and 3(a), which owes to the fact that the response tensors of isotropic media in motion are the same as that of stationary bianisotropic media.[42]

Figure 2 shows the superluminal scenario with $v_{medium} > c/n$. Since the swift electron and the medium move toward two reversed directions, the electron velocity $v_e' = \frac{v_e+v_{medium}}{1+v_e v_{medium}/c^2}$ under the medium co-moving frame S' would increase monotonically with v_e. This way, we have the following inequality:

$$v_e' \ge \min\left(\frac{v_e + v_{medium}}{1+v_e v_{medium}/c^2}\right) = \frac{v_e + v_{medium}}{1+v_e v_{medium}/c^2}\bigg|_{v_e=0} = v_{medium}. \tag{7}$$

Since $v_{medium} > c/n$, Eq. (7) can be transformed into

$$v_e' > c/n \quad \text{for} \quad \forall v_e \in [0, c], \quad \text{if} \quad v_{medium} > c/n. \tag{8}$$

Moreover, since $c/n = c/n \cdot \frac{c/n}{c/n} > c/n \cdot \frac{c/n}{v_{medium}} = c^2/n^2 v_{medium}$, Eq. (8) can be re-written as

$$v_e' > c^2/n^2 v_{medium} \quad \text{for} \quad \forall v_e \in [0, c], \quad \text{if} \quad v_{medium} > c/n. \tag{9}$$

Equation (9) exactly corresponds to the necessary and sufficient condition to enable the emergence of reversed Cherenkov radiation in Eq. (3). Essentially, Eq. (9) indicates that under the static laboratory frame S, when the medium moves superluminally with $v_{medium} > c/n$, the reversed Cherenkov radiation can occur for arbitrary electron velocity v_e and is thus thresholdless for the electron velocity.

This thresholdless feature can be further verified through the isofrequency contour analysis of eigenmodes of light in moving media in Fig. 2(a). By enforcing the momentum-matching condition between the swift electron and the emitted light along the $\hat{z}$ direction, the wavevector of emitted light under the frame S has $k_z = \hat{z}\cdot\bar{k} = -\omega/v_e$. Since $0 \le v_e \le c$, these emitted light always has $k_z \le -\omega/c$. For eigenmodes with $k_z \le -\omega/c$ in Fig. 2(a), their group velocity always has $v_{g,z} > 0$. Under this scenario, the emitted light always has $\bar{v}_g \cdot \bar{v}_e = (\hat{z}v_{g,z})\cdot(-\hat{z}v_e) < 0$ and thus $\theta > 90°$ in Figs. 2(b) and 2(c) for arbitrary electron velocity v_e, indicating the occurrence of thresholdless reversed Cherenkov radiation under the frame S.

Figures 3 and 4 show the subluminal scenario with $c/n^2 < v_{\mathrm{medium}} < c/n$. Under this scenario, we find the existence of electron velocity threshold $v_{\mathrm{th,rCR,e}}$ for the reversed Cherenkov radiation in Figs. 3(a)–3(c), which is dependent on the medium velocity v_{medium}. Recall the two facts that the necessary and sufficient condition to induce the reversed Cherenkov radiation is $v'_{\mathrm{e}} > c^2/n^2 v_{\mathrm{medium}}$, as governed by Eq. (3), and meanwhile, that the electron velocity $v_{\mathrm{e}} = \frac{v'_{\mathrm{e}} - v_{\mathrm{medium}}}{1 - v'_{\mathrm{e}} v_{\mathrm{medium}}/c^2}$ under the frame S increases monotonically with v'_{e}. This way, the reversed Cherenkov radiation under the frame S would emerge only if $v_{\mathrm{e}} > v_{\mathrm{th,rCR,e}}$ (see case 1 in Fig. 4), where

$$v_{\mathrm{th,rCR,e}} = \left. \frac{v'_{\mathrm{e}} - v_{\mathrm{medium}}}{1 - v'_{\mathrm{e}} v_{\mathrm{medium}}/c^2} \right|_{v'_{\mathrm{e}} = c^2/n^2 v_{\mathrm{medium}}} = \frac{1/n^2 - v^2_{\mathrm{medium}}/c^2}{(1 - 1/n^2) v_{\mathrm{medium}}/c} c. \tag{10}$$

According to Eq. (10), $v_{\mathrm{th,rCR,e}}$ would decrease from c to 0 when the medium velocity v_{medium} increases from c/n^2 to c/n, as shown in Figs. 3(b) and 3(c). This is consistent with the isofrequency contour analysis in Fig. 3(a), where the emitted light would have $v_{g,z} > 0$ if $-\omega/v_{\mathrm{th,rCR,e}} < k_z = -\omega/v_{\mathrm{e}} \le -\omega/c$ (i.e., $v_{\mathrm{th,rCR,e}} < v_{\mathrm{e}} \le c$).

Similarly, we also find the existence of electron velocity threshold $v_{\mathrm{th,CR,e}}$ for conventional Cherenkov radiation, since the necessary and sufficient condition for its emergence requires $v'_{\mathrm{e}} > c/n$. This way, the conventional Cherenkov radiation under the frame S would emerge only if $v_{\mathrm{e}} > v_{\mathrm{th,CR,e}}$ (see cases 2 and 3 in Fig. 4), where

$$v_{\mathrm{th,CR,e}} = \left. \frac{v'_{\mathrm{e}} - v_{\mathrm{medium}}}{1 - v'_{\mathrm{e}} v_{\mathrm{medium}}/c^2} \right|_{v'_{\mathrm{e}} = c/n} = \frac{1/n - v_{\mathrm{medium}}/c}{1 - 1/n \cdot v_{\mathrm{medium}}/c} c. \tag{11}$$

According to Eq. (11), $v_{\mathrm{th,CR,e}}$ would decrease from c/n to 0 when the medium velocity v_{medium} increases from 0 to c/n in Figs. 3(b) and 3(c).

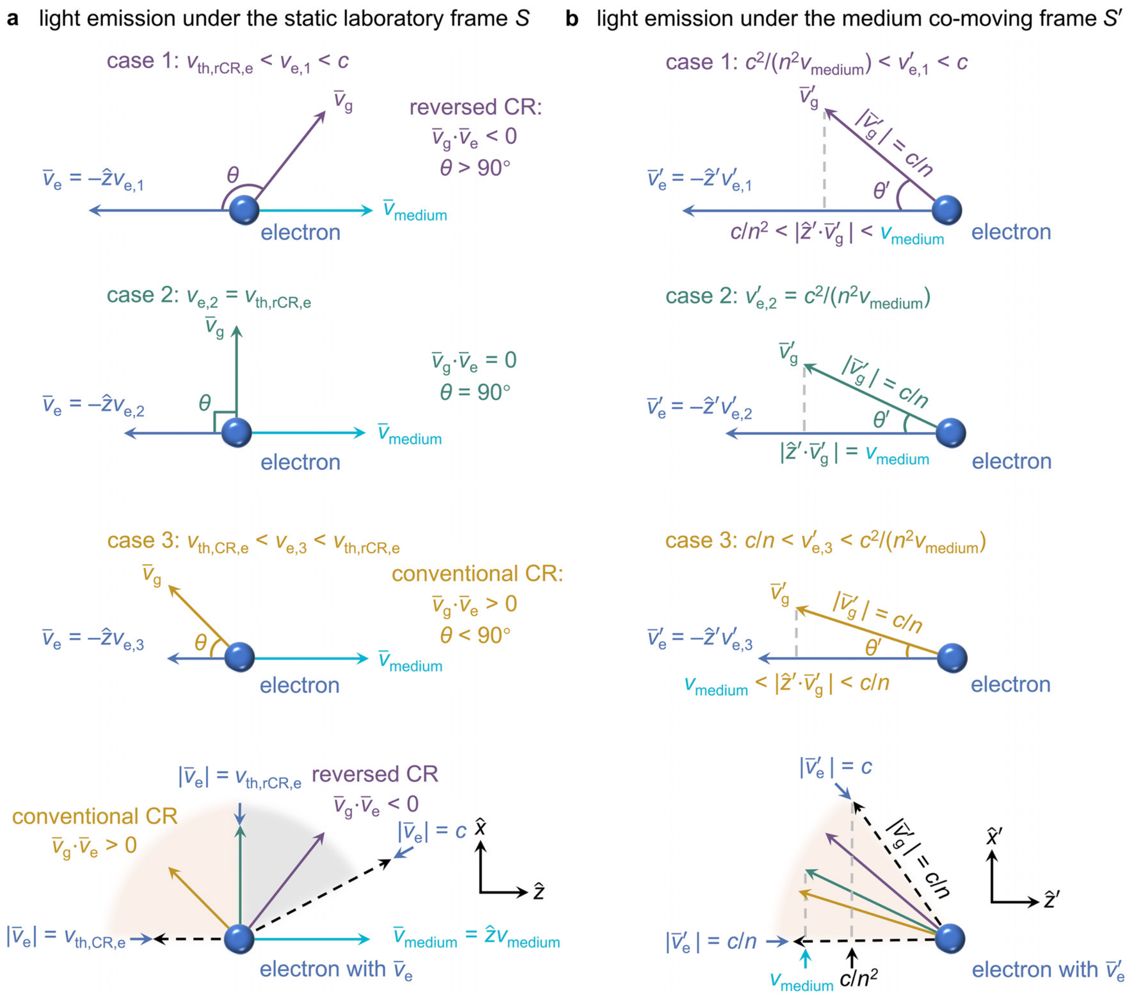

FIG. 4. Underlying mechanism of reversed Cherenkov radiation inside subluminal moving media with $c/n^2 < v_{\mathrm{medium}} < c/n$ under the laboratory frame S. (a) Light emission under the static laboratory frame S. For case 1 with $v_{\mathrm{th,rCR,e}} < v_{\mathrm{e}} = v_{\mathrm{e,1}} < c$, the light emission under the frame S has $\bar{v}_{\mathrm{g}} \cdot \bar{v}_{\mathrm{e}} < 0$ and $\theta > 90°$, which corresponds to the reversed Cherenkov radiation. For case 2 with $v_{\mathrm{e}} = v_{\mathrm{e,2}} = v_{\mathrm{th,rCR,e}}$, the light emission under the frame S has $\bar{v}_{\mathrm{g}} \cdot \bar{v}_{\mathrm{e}} = 0$ and $\theta = 90°$. For case 3 with $v_{\mathrm{th,CR,e}} < v_{\mathrm{e}} = v_{\mathrm{e,3}} < v_{\mathrm{th,rCR,e}}$, the light emission under the frame S has $\bar{v}_{\mathrm{g}} \cdot \bar{v}_{\mathrm{e}} > 0$ and $\theta < 90°$, which corresponds to the conventional Cherenkov radiation. (b) Light emission under the medium co-moving frame S'. For comparison, each case under the frame S in (a) is correspondingly re-plotted under the frame S' in (b).

Under this scenario, the emitted light always has $v_{g,z} < 0$ if $-\omega/v_{\mathrm{th,CR,e}} < k_z = -\omega/v_e < -\omega/v_{\mathrm{th,rCR,e}}$ (i.e., $v_{\mathrm{th,CR,e}} < v_e < v_{\mathrm{th,rCR,e}}$), as shown in Fig. 3(a).

In conclusion, we have revealed the possibility to create the reversed Cherenkov radiation from positive-index moving media by exploiting the Fizeau–Fresnel drag effect. Remarkably, we have discovered the existence of medium velocity threshold for the creation of reversed Cherenkov radiation, namely, $v_{\mathrm{th,rCR,medium}} = c/n^2$, which is solely determined by the medium's refractive index. Specifically, we have further found that the reversed Cherenkov radiation becomes thresholdless for the charged particle velocity when the medium moves superluminally. We highlight that the moving media, in principle, could be effectively constructed, for example, by using spatiotemporal materials,[89–101] nonreciprocal graphene or metal biased with a drift current,[102–109] and nonlinear materials under the illumination of laser pulses.[110–112] Due to the rich un-explored physics in the realm of light–particle–matter interactions, our finding may spark the continuous exploration of free-electron radiation (including reversed Cherenkov radiation) in more complex yet exotic photonic systems, such as spatiotemporal materials, nonreciprocal metasurfaces, and nonlinear materials.

See the supplementary material for five sections, including derivation of Cherenkov radiation under the medium co-moving frame S', derivation of Cherenkov radiation under the static laboratory frame S, derivation of dispersion relation for moving isotropic media, derivation of the radiation angle θ under the static laboratory frame S, and more discussion on the reversed Cherenkov radiation via Fizeau–Fresnel drag.

X.L. acknowledges the support partly from the National Natural Science Foundation of China (NSFC) under Grant No. 62475227, the National Natural Science Foundation of China (NSFC) under Grant No. 62175212, the Zhejiang Provincial Natural Science Fund Key Project under Grant No. LZ23F050003, and Fundamental Research Funds for the Central Universities under Grant No. 226-2024-00022. H.C. acknowledges the support from the Key Research and Development Program of the Ministry of Science and Technology under Grant No. 2022YFA1404704, the Key Research and Development Program of the Ministry of Science and Technology under Grant No. 2022YFA1405200, the Key Research and Development Program of the Ministry of Science and Technology under Grant No. 2022YFA1404902, the Key Research and Development Program of Zhejiang Province under Grant No.2022C01036, and Fundamental Research Funds for the Central Universities. R.C. acknowledges the support partly from the National Natural Science Foundation of China (NSFC) under Grant No. 623B2089. Y.Y. acknowledges the support from the National Natural Science Foundation of China Excellent Young Scientists Fund (Grant No. HKU 12222417), Hong Kong Research Grant Council Strategic Topics, Grant No. STG3/E-704/23-N, the startup fund of the University of Hong Kong, and the Asian Young Scientist Fellowship.

AUTHOR DECLARATIONS

Conflict of Interest

The authors have no conflicts to disclose.

Author Contributions

Bowen Zhang and Zheng Gong contributed equally to this work.

Bowen Zhang: Conceptualization (equal); Investigation (equal); Visualization (equal); Writing – original draft (equal). **Zheng Gong:** Investigation (equal); Visualization (equal); Writing – review & editing (equal). **Ruoxi Chen:** Visualization (equal); Writing – review & editing (equal). **Xuhuinan Chen:** Visualization (equal); Writing – review & editing (equal). **Yi Yang:** Visualization (equal); Writing – review & editing (equal). **Hongsheng Chen:** Supervision (equal); Visualization (equal); Writing – review & editing (equal). **Ido Kaminer:** Supervision (equal); Visualization (equal); Writing – review & editing (equal). **Xiao Lin:** Conceptualization (equal); Supervision (equal); Visualization (equal); Writing – original draft (equal).

DATA AVAILABILITY

The data that support the findings of this study are available within the article and its supplementary material.

REFERENCES

[1]Y. Yang, J.-W. Henke, A. S. Raja, F. J. Kappert, G. Huang, G. Arend, Z. Qiu, A. Feist, R. N. Wang, A. Tusnin, A. Tikan, C. Ropers, and T. J. Kippenberg, "Free-electron interaction with nonlinear optical states in microresonators," Science **383**, 168 (2024).
[2]F. Tay, X. Lin, X. Shi, H. Chen, I. Kaminer, and B. Zhang, "Bulk-plasmon-mediated free-electron radiation beyond the conventional formation time," Adv. Sci. **10**, 2300760 (2023).
[3]D. Zhang, Y. Zeng, Y. Bai, Z. Li, Y. Tian, and R. Li, "Coherent surface plasmon polariton amplification via free-electron pumping," Nature **611**, 55 (2022).
[4]A. Gonoskov, T. G. Blackburn, M. Marklund, and S. S. Bulanov, "Charged particle motion and radiation in strong electromagnetic fields," Rev. Mod. Phys. **94**, 045001 (2022).
[5]X. Lin and B. Zhang, "Normal Doppler frequency shift in negative refractive-index systems," Laser Photonics Rev. **13**, 1900081 (2019).
[6]X. Shi, X. Lin, I. Kaminer, F. Gao, Z. Yang, J. D. Joannopoulos, M. Soljačić, and B. Zhang, "Superlight inverse Doppler effect," Nat. Phys. **14**, 1001 (2018).
[7]Y. Yang, A. Massuda, C. Roques-Carmes, S. E. Kooi, T. Christensen, S. G. Johnson, J. D. Joannopoulos, O. D. Miller, I. Kaminer, and M. Soljačić, "Maximal spontaneous photon emission and energy loss from free electrons," Nat. Phys. **14**, 894 (2018).
[8]G. Li, T. Zentgraf, and S. Zhang, "Rotational Doppler effect in nonlinear optics," Nat. Phys. **12**, 736 (2016).
[9]X. Lin, I. Kaminer, X. Shi, F. Gao, Z. Yang, Z. Gao, H. Buljan, J. D. Joannopoulos, M. Soljačić, H. Chen, and B. Zhang, "Splashing transients of 2D plasmons launched by swift electrons," Sci. Adv. **3**, e1601192 (2017).
[10]A. J. Macleod, A. Noble, and D. A. Jaroszynski, "Cherenkov radiation from the quantum vacuum," Phys. Rev. Lett. **122**, 161601 (2019).
[11]I. Kaminer, Y. T. Katan, H. Buljan, Y. Shen, O. Ilic, J. J. López, L. J. Wong, J. D. Joannopoulos, and M. Soljačić, "Efficient plasmonic emission by the quantum Čerenkov effect from hot carriers in graphene," Nat. Commun. **7**, 11880 (2016).
[12]F. J. G. de Abajo, "Optical excitations in electron microscopy," Rev. Mod. Phys. **82**, 209 (2010).
[13]Y. Zhang, Z. D. Gao, Z. Qi, S. N. Zhu, and N. B. Ming, "Nonlinear Čerenkov radiation in nonlinear photonic crystal waveguides," Phys. Rev. Lett. **100**, 163904 (2008).
[14]T. Li, F. Liu, Y. Chen, X. Xiong, K. Cui, X. Feng, W. Zhang, and Y. Huang, "On-chip Cherenkov radiation tuning in 3.2–14 THz," Nat. Commun. **16**, 7921 (2025).
[15]Z. Xie, X. Lin, S. Zhu, C. Huang, Y. Luo, and H. Hu, "Transverse-electric Cherenkov radiation for TeV-scale particle detection," arXiv:2508.20896 (2025).

[16]Z. Xu, S. Bao, J. Liu, J. Chang, X. Kong, V. Galdi, and T. J. Cui, "Observation of analog flatland Cherenkov radiations on metasurfaces," Laser Photonics Rev. **18**, 2300763 (2024).
[17]H. Hu, X. Lin, D. Liu, H. Chen, B. Zhang, and Y. Luo, "Broadband enhancement of Cherenkov radiation using dispersionless plasmons," Adv. Sci. **9**, 2200538 (2022).
[18]P. Genevet, D. Wintz, A. Ambrosio, A. She, R. Blanchard, and F. Capasso, "Controlled steering of Cherenkov surface plasmon wakes with a one-dimensional metamaterial," Nat. Nanotechnol. **10**, 804 (2015).
[19]Y. Adiv, H. Hu, S. Tsesses, R. Dahan, K. Wang, Y. Kurman, A. Gorlach, H. Chen, X. Lin, G. Bartal, and I. Kaminer, "Observation of 2D Cherenkov radiation," Phys. Rev. X **13**, 011002 (2023).
[20]C. Wang, X. Chen, Z. Gong, R. Chen, H. Hu, H. Wang, Y. Yang, L. Tony, B. Zhang, H. Chen, and X. Lin, "Superscattering of light: Fundamentals and applications," Rep. Prog. Phys. **87**, 126401 (2024).
[21]C. Roques-Carmes, S. E. Kooi, Y. Yang, N. Rivera, P. D. Keathley, J. D. Joannopoulos, S. G. Johnson, I. Kaminer, K. K. Berggren, and M. Soljačić, "Free-electron–light interactions in nanophotonics," Appl. Phys. Rev. **10**, 011303 (2023).
[22]N. Rivera and I. Kaminer, "Light-matter interactions with photonic quasiparticles," Nat. Rev. Phys. **2**, 538 (2020).
[23]H. Hu, X. Lin, and Y. Luo, "Free-electron radiation engineering via structured environments," PIER **171**, 75 (2021).
[24]J. J. Aubert, U. Becker, P. J. Biggs, J. Burger, M. Chen, G. Everhart, P. Goldhagen, J. Leong, T. McCorriston, T. G. Rhoades, M. Rohde, S. C. C. Ting, S. L. Wu, and Y. Y. Lee, "Experimental observation of a heavy particle J," Phys. Rev. Lett. **33**, 1404 (1974).
[25]O. Chamberlain, E. Segrè, C. Wiegand, and T. Ypsilantis, "Observation of antiprotons," Phys. Rev. **100**, 947 (1955).
[26]M. Amenomori *et al.*, "First detection of sub-PeV diffuse gamma rays from the galactic disk: Evidence for ubiquitous galactic cosmic rays beyond PeV Energies," Phys. Rev. Lett. **126**, 141101 (2021).
[27]V. Ginis, J. Danckaert, I. Veretennicoff, and P. Tassin, "Controlling Cherenkov radiation with transformation-optical metamaterials," Phys. Rev. Lett. **113**, 167402 (2014).
[28]X. Lin, H. Hu, S. Easo, Y. Yang, Y. Shen, K. Yin, M. P. Blago, I. Kaminer, B. Zhang, H. Chen, J. Joannopoulos, M. Soljačić, and Y. Luo, "A Brewster route to Cherenkov detectors," Nat. Commun. **12**, 5554 (2021).
[29]H. Hu, X. Lin, L. J. Wong, Q. Yang, D. Liu, B. Zhang, and Y. Luo, "Surface Dyakonov–Cherenkov radiation," eLight **2**, 2 (2022).
[30]F. Liu, L. Xiao, Y. Ye, M. Wang, K. Cui, X. Feng, W. Zhang, and Y. Huang, "Integrated Cherenkov radiation emitter eliminating the electron velocity threshold," Nat. Photonics **11**, 289 (2017).
[31]S. Liu, P. Zhang, W. Liu, S. Gong, R. Zhong, Y. Zhang, and M. Hu, "Surface polariton Cherenkov light radiation source," Phys. Rev. Lett. **109**, 153902 (2012).
[32]L. J. Wong, I. Kaminer, O. Ilic, J. D. Joannopoulos, and M. Soljačić, "Towards graphene plasmon-based free-electron infrared to X-ray sources," Nat. Photonics **10**, 46 (2016).
[33]G. Adamo, K. F. MacDonald, Y. H. Fu, C. M. Wang, D. P. Tsai, F. J. G. de Abajo, and N. I. Zheludev, "Light well: A tunable free-electron light source on a chip," Phys. Rev. Lett. **103**, 113901 (2009).
[34]T. M. Shaffer, E. C. Pratt, and J. Grimm, "Utilizing the power of Cerenkov light with nanotechnology," Nat. Nanotechnol. **12**, 106 (2017).
[35]D. A. Alexander, A. Nomezine, L. A. Jarvis, D. J. Gladstone, B. W. Pogue, and P. Bruza, "Color Cherenkov imaging of clinical radiation therapy," Light **10**, 226 (2021).
[36]R. L. Hachadorian, P. Bruza, M. Jermyn, D. J. Gladstone, B. W. Pogue, and L. A. Jarvis, "Imaging radiation dose in breast radiotherapy by X-ray CT calibration of Cherenkov light," Nat. Commun. **11**, 2298 (2020).
[37]A. Kamkaew, L. Cheng, S. Goel, H. F. Valdovinos, T. E. Barnhart, Z. Liu, and W. Cai, "Cerenkov radiation induced photodynamic therapy using chlorin e6-loaded hollow mesoporous silica nanoparticles," ACS Appl. Mater. Interfaces **8**, 26630 (2016).
[38]N. Kotagiri, G. P. Sudlow, W. J. Akers, and S. Achilefu, "Breaking the depth dependency of phototherapy with Cerenkov radiation and low-radiance-responsive nanophotosensitizers," Nat. Nanotechnol. **10**, 370 (2015).
[39]X. Wang, L. Li, J. Li, P. Wang, J. Lang, and Y. Yang, "Cherenkov luminescence in tumor diagnosis and treatment: A Review," Photonics **9**, 390 (2022).
[40]P. A. Cherenkov, "Visible emission of clean liquids by action of γ radiation," Dokl. Akad. Nauk SSSR **2**, 451 (1934).
[41]I. E. Tamm and I. M. Frank, "Coherent radiation of fast electrons in a medium," Dokl. Akad. Nauk SSSR **14**, 107 (1937).
[42]J. A. Kong, *Electromagnetic Wave Theory* (EMW Publishing, 2008).
[43]V. G. Veselago, "Electrodynamics of substances with simultaneously negative values of ε and μ," Sov. Phys. Usp. **10**, 509 (1968).
[44]D. V. Skryabin, Y. V. Kartashov, O. A. Egorov, M. Sich, J. K. Chana, L. E. T. Rodriguez, P. M. Walker, E. Clarke, B. Royall, M. S. Skolnick, and D. N. Krizhanovskii, "Backward Cherenkov radiation emitted by polariton solitons in a microcavity wire," Nat. Commun. **8**, 1554 (2017).
[45]S. N. Galyamin, A. V. Tyukhtin, A. Kanareykin, and P. Schoessow, "Reversed Cherenkov-transition radiation by a charge crossing a left-handed medium boundary," Phys. Rev. Lett. **103**, 194802 (2009).
[46]O. J. Franca, L. F. Urrutia, and O. Rodríguez-Tzompantzi, "Reversed electromagnetic Vavilov-Čerenkov radiation in naturally existing magnetoelectric media," Phys. Rev. D **99**, 116020 (2019).
[47]H. Chen and M. Chen, "Flipping photons backward: Reversed Cherenkov radiation," Mater. Today **14**, 34 (2011).
[48]S. Xi, H. Chen, T. Jiang, L. Ran, J. Huangfu, B.-I. Wu, J. A. Kong, and M. Chen, "Experimental verification of reversed Cherenkov radiation in left-handed metamaterial," Phys. Rev. Lett. **103**, 194801 (2009).
[49]S. Antipov, L. Spentzouris, W. Gai, M. Conde, F. Franchini, R. Konecny, W. Liu, J. G. Power, Z. Yusof, and C. Jing, "Observation of wakefield generation in left-handed band of metamaterial-loaded waveguide," J. Appl. Phys. **104**, 014901 (2008).
[50]Z. Duan, X. Tang, Z. Wang, Y. Zhang, X. Chen, M. Chen, and Y. Gong, "Observation of the reversed Cherenkov radiation," Nat. Commun. **8**, 14901 (2017).
[51]X. Lu, M. A. Shapiro, I. Mastovsky, R. J. Temkin, M. Conde, J. G. Power, J. Shao, E. E. Wisniewski, and C. Jing, "Generation of high-power, reversed-Cherenkov wakefield radiation in a metamaterial structure," Phys. Rev. Lett. **122**, 014801 (2019).
[52]J. Tao, L. Wu, G. Zheng, and S. Yu, "Cherenkov polaritonic radiation in a natural hyperbolic material," Carbon **150**, 136 (2019).
[53]X. Guo, C. Wu, S. Zhang, D. Hu, S. Zhang, Q. Jiang, X. Dai, Y. Duan, X. Yang, Z. Sun, S. Zhang, H. Xu, and Q. Dai, "Mid-infrared analogue polaritonic reversed Cherenkov radiation in natural anisotropic crystals," Nat. Commun. **14**, 2532 (2023).
[54]S. N. Galyamin and A. V. Tyukhtin, "Electromagnetic field of a charge traveling into an anisotropic medium," Phys. Rev. E **84**, 056608 (2011).
[55]Y. Zhang, C. Hu, B. Lyu, H. Li, Z. Ying, L. Wang, A. Deng, X. Luo, Q. Gao, J. Chen, J. Du, P. Shen, K. Watanabe, T. Taniguchi, J.-H. Kang, F. Wang, Y. Zhang, and Z. Shi, "Tunable Cherenkov radiation of phonon polaritons in silver nanowire/hexagonal boron nitride heterostructures," Nano Lett. **20**, 2770 (2020).
[56]V. G. Veselago and E. E. Narimanov, "The left hand of brightness: Past, present and future of negative index materials," Nat. Mater. **5**, 759 (2006).
[57]R. Chen, Z. Gong, Z. Wang, X. Xi, B. Zhang, Y. Yang, B. Zhang, I. Kaminer, H. Chen, and X. Lin, "A gain route to reversed Cherenkov radiation," Sci. Adv. **11**, eads5113 (2025).
[58]C. Luo, M. Ibanescu, S. G. Johnson, and J. D. Joannopoulos, "Cerenkov radiation in photonic crystals," Science **299**, 368 (2003).
[59]X. Lin, S. Easo, Y. Shen, H. Chen, B. Zhang, J. D. Joannopoulos, M. Soljačić, and I. Kaminer, "Controlling Cherenkov angles with resonance transition radiation," Nat. Phys. **14**, 816 (2018).
[60]Z. Gong, J. Chen, R. Chen, X. Zhu, C. Wang, X. Zhang, H. Hu, Y. Yang, B. Zhang, H. Chen, I. Kaminer, and X. Lin, "Interfacial Cherenkov radiation from ultralow-energy electrons," Proc. Natl. Acad. Sci. U. S. A. **120**, e2306601120 (2023).
[61]F. P. Bretherton and C. J. R. Garrett, "Wavetrains in inhomogeneous moving media," Proc. R. Soc. A **302**, 529 (1968).
[62]A. A. Svidzinsky, F. Li, and X. Zhang, "Generation of coherent light by a moving medium," Phys. Rev. Lett. **118**, 123902 (2017).
[63]M. Artoni, I. Carusotto, G. C. La Rocca, and F. Bassani, "Fresnel light drag in a coherently driven moving medium," Phys. Rev. Lett. **86**, 2549 (2001).

[64]A. Fresnel, "Lettre d'Augustin Fresnel à François Arago sur l'influence du mouvement terrestre dans quelques phénomènes d'optique," Ann. Chim. Phys. **9**, 57 (1818).
[65]M. H. Fizeau, "Sur les hypothèses relatives à l'éther lumineux, et sur une expérience qui parait démontrer que le mouvement des corps change la vitesse avec laquelle la lumière se propage dans leur intérieur," C. R. Acad. Sci. **33**, 349 (1851).
[66]A. Einstein, "Zur elektrodynamik bewegter körper," Ann. Phys. **322**, 891 (1905).
[67]J. D. Jackson, *Classical Electrodynamics* (John Wiley & Sons, 2021).
[68]J. B. Pendry, "Shearing the vacuum - quantum friction," J. Phys.: Condens. Matter **9**, 10301 (1997).
[69]J. B. Pendry, "Can sheared surfaces emit light?," J. Mod. Opt. **45**, 2389 (1998).
[70]A. I. Volokitin and B. N. J. Persson, "Near-field radiative heat transfer and noncontact friction," Rev. Mod. Phys. **79**, 1291 (2007).
[71]G. V. Dedkov and A. A. Kyasov, "Fluctuation-electromagnetic interaction under dynamic and thermal nonequilibrium conditions," Phys-Usp. **60**, 559 (2017).
[72]Z. Gong, R. Chen, Z. Wang, X. Xi, Y. Yang, B. Zhang, H. Chen, I. Kaminer, and X. Lin, "Free-electron resonance transition radiation via Brewster randomness," Proc. Natl. Acad. Sci. U. S. A. **122**, e2413336122 (2025).
[73]J. H. Gaida, H. Lourenco-Martins, M. Sivis, T. Rittmann, A. Feist, F. J. G. de Abajo, and C. Ropers, "Attosecond electron microscopy by free-electron homodyne detection," Nat. Photonics **18**, 509 (2024).
[74]J. Chen, R. Chen, F. Tay, Z. Gong, H. Hu, Y. Yang, X. Zhang, C. Wang, I. Kaminer, H. Chen, B. Zhang, and X. Lin, "Low-velocity-favored transition radiation," Phys. Rev. Lett. **131**, 113002 (2023).
[75]S. Huang, R. Duan, N. Pramanik, M. Go, C. Boothroyd, Z. Liu, and L. J. Wong, "Multicolor x-rays from free electron-driven van der Waals heterostructures," Sci. Adv. **9**, eadj8584 (2023).
[76]R. Chen, Z. Gong, J. Chen, X. Zhang, X. Zhu, H. Chen, and X. Lin, "Recent advances of transition radiation: Fundamentals and applications," Mater. Today Electron. **3**, 100025 (2023).
[77]X.-N. Li, L.-Z. Peng, Y.-Y. Liu, L.-H. Hong, D.-M. Hu, Y.-Y. Zhao, X.-M. Duan, B.-Q. Chen, and Z.-Y. Li, "Nonlinear Raman-Nath diffraction in submicron-thick periodically poled lithium niobate thin film," PhotoniX **5**, 42 (2024).
[78]X. Lin and H. Chen, "Shaping free-electron radiation via van der Waals heterostructures," Light **12**, 187 (2023).
[79]M. Shentcis, A. K. Budniak, X. Shi, R. Dahan, Y. Kurman, M. Kalina, H. Herzig Sheinfux, M. Blei, M. K. Svendsen, Y. Amouyal, S. Tongay, K. S. Thygesen, F. H. L. Koppens, E. Lifshitz, F. J. García de Abajo, L. J. Wong, and I. Kaminer, "Tunable free-electron X-ray radiation from van der Waals materials," Nat. Photonics **14**, 686 (2020).
[80]R. Chen, J. Chen, Z. Gong, X. Zhang, X. Zhu, Y. Yang, I. Kaminer, H. Chen, B. Zhang, and X. Lin, "Free-electron Brewster-transition radiation," Sci. Adv. **9**, eadh8098 (2023).
[81]M. Henstridge, C. Pfeiffer, D. Wang, A. Boltasseva, V. M. Shalaev, A. Grbic, and R. Merlin, "Synchrotron radiation from an accelerating light pulse," Science **362**, 439 (2018).
[82]C. T. Tai, "A study of electrodynamics of moving media," Proc. IEEE **52**, 685 (1964).
[83]B. M. Bolotovskiĭ and S. N. Stolyarov, "Current status of the electrodynamics of moving media (infinite media)," Sov. Phys. Usp. **17**, 875 (1975).
[84]B. M. Bolotovskiĭ and S. N. Stolyarov, "Radiation from and energy loss by charged particles in moving media," Sov. Phys. Usp. **35**, 143 (1992).
[85]T. M. Grzegorczyk and J. A. Kong, "Electrodynamics of moving media inducing positive and negative refraction," Phys. Rev. B **74**, 033102 (2006).
[86]U. Leonhardt and P. Piwnicki, "Relativistic effects of light in moving media with extremely low group velocity," Phys. Rev. Lett. **84**, 822 (2000).
[87]M. G. Silveirinha, "Quantization of the electromagnetic field in nondispersive polarizable moving media above the Cherenkov threshold," Phys. Rev. A **88**, 043846 (2013).
[88]Z. L. Wang and J. Shao, "Recent progress on the Maxwell's equations for describing a mechano-driven medium system with multiple moving objects/media," Electromag. Sci. **1**, 1 (2023).
[89]X. Wang, M. S. Mirmoosa, V. S. Asadchy, C. Rockstuhl, S. Fan, and S. A. Tretyakov, "Metasurface-based realization of photonic time crystals," Sci. Adv. **9**, eadg7541 (2023).
[90]Z.-L. Deck-Léger, N. Chamanara, M. Skorobogatiy, M. G. Silveirinha, and C. Caloz, "Uniform-velocity spacetime crystals," Adv. Photonics **1**, 1 (2019).
[91]X. Wang, P. Garg, M. S. Mirmoosa, A. G. Lamprianidis, C. Rockstuhl, and V. S. Asadchy, "Expanding momentum bandgaps in photonic time crystals through resonances," Nat. Photonics **19**, 149 (2025).
[92]M. Camacho, B. Edwards, and N. Engheta, "Achieving asymmetry and trapping in diffusion with spatiotemporal metamaterials," Nat. Commun. **11**, 3733 (2020).
[93]Z. Chen, Y. Peng, H. Li, J. Liu, Y. Ding, B. Liang, X.-F. Zhu, Y. Lu, J. Cheng, and A. Alù, "Efficient nonreciprocal mode transitions in spatiotemporally modulated acoustic metamaterials," Sci. Adv. **7**, eabj1198 (2021).
[94]J. Dong, S. Zhang, H. He, H. Li, and J. Xu, "Nonuniform wave momentum band gap in biaxial anisotropic photonic time crystals," Phys. Rev. Lett. **134**, 063801 (2025).
[95]P. A. Huidobro, E. Galiffi, S. Guenneau, R. V. Craster, and J. B. Pendry, "Fresnel drag in space-time-modulated metamaterials," Proc. Natl. Acad. Sci. U. S. A. **116**, 24943 (2019).
[96]E. Galiffi, R. Tirole, S. Yin, H. Li, S. Vezzoli, P. A. Huidobro, M. G. Silveirinha, R. Sapienza, A. Alu, and J. B. Pendry, "Photonics of time-varying media," Adv. Photonics **4**, 014002 (2022).
[97]Z. Gong, R. Chen, H. Chen, and X. Lin, "Anomalous Maxwell-Garnett theory for photonic time crystals," Appl. Phys. Rev. **12**, 031414 (2025).
[98]H. Li, S. Yin, H. He, J. Xu, A. Alù, and B. Shapiro, "Stationary charge radiation in anisotropic photonic time crystals," Phys. Rev. Lett. **130**, 093803 (2023).
[99]P. A. Huidobro, M. G. Silveirinha, E. Galiffi, and J. B. Pendry, "Homogenization theory of space-time metamaterials," Phys. Rev. Appl. **16**, 014044 (2021).
[100]J. C. Serra and M. G. Silveirinha, "Homogenization of dispersive space-time crystals: Anomalous dispersion and negative stored energy," Phys. Rev. B **108**, 035119 (2023).
[101]F. R. Prudêncio and M. G. Silveirinha, "Replicating physical motion with Minkowskian isorefractive spacetime crystals," Nanophotonics **12**, 3007 (2023).
[102]T. A. Morgado and M. G. Silveirinha, "Negative Landau damping in bilayer graphene," Phys. Rev. Lett. **119**, 133901 (2017).
[103]T. A. Morgado and M. G. Silveirinha, "Drift-induced unidirectional graphene plasmons," ACS Photonics **5**, 4253 (2018).
[104]T. A. Morgado and M. G. Silveirinha, "Nonlocal effects and enhanced nonreciprocity in current-driven graphene systems," Phys. Rev. B **102**, 075102 (2020).
[105]W. Zhao, S. Zhao, H. Li, S. Wang, S. Wang, M. I. B. Utama, S. Kahn, Y. Jiang, X. Xiao, S. Yoo, K. Watanabe, T. Taniguchi, A. Zettl, and F. Wang, "Efficient Fizeau drag from Dirac electrons in monolayer graphene," Nature **594**, 517 (2021).
[106]Y. Dong, L. Xiong, I. Y. Phinney, Z. Sun, R. Jing, A. S. McLeod, S. Zhang, S. Liu, F. L. Ruta, H. Gao, Z. Dong, R. Pan, J. H. Edgar, P. Jarillo-Herrero, L. S. Levitov, A. J. Millis, M. M. Fogler, D. A. Bandurin, and D. N. Basov, "Fizeau drag in graphene plasmonics," Nature **594**, 513 (2021).
[107]M. G. Blevins and S. V. Boriskina, "Plasmon Fizeau drag in 3D Dirac and Weyl semimetals," ACS Photonics **11**, 537 (2024).
[108]K. Y. Bliokh, F. J. Rodríguez-Fortuño, A. Y. Bekshaev, Y. S. Kivshar, and F. Nori, "Electric-current-induced unidirectional propagation of surface plasmon-polaritons," Opt. Lett. **43**, 963 (2018).
[109]S. A. H. Gangaraj and F. Monticone, "Drifting electrons: Nonreciprocal plasmonics and thermal photonics," ACS Photonics **9**, 806 (2022).
[110]O. Reshef, I. De Leon, M. Z. Alam, and R. W. Boyd, "Nonlinear optical effects in epsilon-near-zero media," Nat. Rev. Mater. **4**, 535 (2019).
[111]K. Xia, F. Nori, and M. Xiao, "Cavity-free optical isolators and circulators using a chiral cross-Kerr nonlinearity," Phys. Rev. Lett. **121**, 203602 (2018).
[112]L. Tang, "Quantum squeezing induced optical nonreciprocity," Phys. Rev. Lett. **128**, 083604 (2022).

Supplementary Information for

Reversed Cherenkov radiation via Fizeau-Fresnel drag

Bowen Zhang, Zheng Gong, Ruoxi Chen, Xuhuinan Chen, Yi Yang, Hongsheng Chen, Ido Kaminer, and Xiao Lin

Supplementary Information Guide:

<u>Section S1: Cherenkov radiation under the medium co-moving frame S'</u>

In this section, we begin with the analysis of conventional Cherenkov radiation under the medium co-moving frame S' using Green's function method [42]. The notation and schematic are consistent with Fig. 1(c) in the main text. Under the frame S', the medium is isotropic and nondispersive with a constant positive refractive index n $(n > 1)$. Here, without loss of generality, the source of radiation is a swift electron with a charge of q, which moves with a velocity of $\bar{v}'_{\mathrm{e}} = -\hat{z}'v'_{\mathrm{e}}$ in Fig. S1.

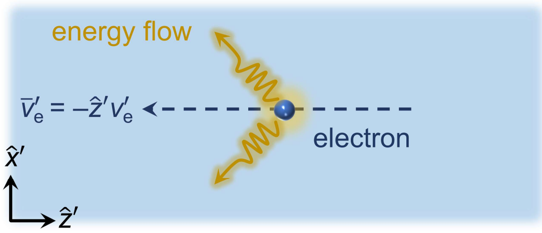

FIG. S1. Schematic of Cherenkov radiation under the medium co-moving frame S'. The electron moves with a velocity of $\bar{v}'_{\mathrm{e}} = -\hat{z}'v'_{\mathrm{e}}$, the refractive index of the medium is set to be n.

From the Maxwell equations, we have

$$\nabla' \times \bar{E}'(\bar{r}', t') = -\mu_0\mu_r \frac{\partial \bar{H}'(\bar{r}', t')}{\partial t'} \tag{S1}$$

$$\nabla' \times \bar{H}'(\bar{r}', t') = \bar{J}'(\bar{r}', t') + \varepsilon_0\varepsilon_{\mathrm{r}} \frac{\partial}{\partial t'} \bar{E}'(\bar{r}', t') \tag{S2}$$

where ε_0 and μ_0 is the permittivity and the permeability of the vacuum, respectively; ε_r and μ_{r} is the relative permittivity and the relative permeability of the medium, respectively. Note that since we are studying a non-magnetic medium, it is assumed that $\mu_{\mathrm{r}} = 1$. Taking the curl of both sides of equation (S1) and substituting equation (S2) into equation (S1), we can obtain the wave equation as

$$\nabla' \times \nabla' \times \bar{E}'(\bar{r}', t') + \varepsilon\mu \frac{\partial^2 \bar{E}'(\bar{r}', t')}{\partial t'^2} = -\mu \frac{\partial \bar{J}'(\bar{r}', t')}{\partial t'} \tag{S3}$$

where $\varepsilon = \varepsilon_0\varepsilon_r$ and $\mu = \mu_0\mu_{\mathrm{r}}$. To solve for the $\bar{E}'(\bar{r}', t')$, we need to know the current density $\bar{J}'(\bar{r}', t')$, which, under this case, can be expressed as

$$\bar{J}'(\bar{r}', t') = \hat{z}'qv'_{\mathrm{e}}\delta(x')\delta(y')\delta(z' + v'_{\mathrm{e}}t') \tag{S4}$$

Since Cherenkov radiation exhibits ϕ' symmetry in cylindrical coordinate system, we transform equation (S4) into cylindrical coordinate system. Note that

$$\int d\rho'\delta(\rho') = 1 = \iint dx'dy'\delta(x')\delta(y') = \int 2\pi\rho' d\rho'\delta(x')\delta(y') \tag{S5}$$

we have

$$\delta(x')\delta(y') = \frac{1}{2\pi\rho'}\delta(\rho') \tag{S6}$$

Thus, equation (S4) can be transformed into cylindrical coordinate system as

$$\bar{J}'(\bar{r}',t') = \hat{z}' q v_{\mathrm{e}}' \delta(z' + v_{\mathrm{e}}' t')\frac{\delta(\rho')}{2\pi\rho'} \tag{S7}$$

Since this source is not time harmonic, we transform equation (S3) and equation (S7) into frequency domain and solve this partial differential equation using Green's function method. The Fourier transform of the electric field and the current source can be expressed as

$$\bar{E}'(\bar{r}',\omega') = \frac{1}{2\pi}\int dt'\, \bar{E}'(\bar{r}',t') e^{i\omega' t'} \tag{S8}$$

$$\bar{J}'(\bar{r}',\omega') = \frac{1}{2\pi}\int dt \bar{J}'(\bar{r}',t') e^{i\omega' t'} = \hat{z}'\frac{q}{4\pi^2\rho'} e^{-i\omega' z'/v_{\mathrm{e}}'}\delta(\rho') \tag{S9}$$

Conversely, the time-domain values can be obtained by inverse Fourier transform as

$$\bar{E}'(\bar{r}',t') = \int d\omega' \bar{E}'(\bar{r}',\omega') e^{-i\omega' t'} \tag{S10}$$

$$\bar{J}'(\bar{r}',t') = \int d\omega' \bar{J}'(\bar{r}',\omega') e^{-i\omega' t'} \tag{S11}$$

By substituting equations (S9)-(S11) into equation (S3) and using dispersion relation $k'^2 = \omega'^2\varepsilon\mu$, we can obtain the wave equation under frequency domain as

$$\nabla' \times \nabla' \times \bar{E}'(\bar{r}',\omega') - k'^2 \bar{E}'(\bar{r}',\omega') = i\omega'\mu \bar{J}'(\bar{r}',\omega') = \hat{z}'\frac{i\omega'\mu q}{4\pi^2\rho'} e^{-i\omega' z'/v_{\mathrm{e}}'}\delta(\rho') \tag{S12}$$

Here, we define a vector Green's function $\bar{g}'(\rho',z')$ and let

$$\bar{E}'(\bar{r}',\omega') = \left[\bar{\bar{I}} + \frac{1}{k'^2}\nabla'\nabla'\right]\cdot \bar{g}'(\rho',z') = \bar{g}'(\rho',z') + \frac{1}{k'^2}\nabla'[\nabla'\cdot\bar{g}'(\rho',z')] \tag{S13}$$

Substituting equation (S13) into equation (S12) and after some calculations, we have the wave function for $\bar{g}'(\rho',z')$ as

$$(\nabla'^2 + k'^2)\bar{g}'(\rho', z') = -\hat{z}'\frac{i\omega'\mu q}{4\pi^2\rho'}e^{-i\omega' z'/v_e'}\delta(\rho') \tag{S14}$$

We can further simplify equation (S14) by defining a scalar Green's function $g'(\rho')$ and letting

$$\bar{g}'(\rho', z') = \hat{z}' g'(\rho')\frac{i\omega'\mu q}{2\pi}e^{-i\omega' z'/v_e'} \tag{S15}$$

Then we obtain

$$\left[\frac{1}{\rho'}\frac{d}{d\rho'}\left(\rho'\frac{d}{d\rho'}\right) - \frac{\omega'^2}{v_e'^2} + k'^2\right]g(\rho') = -\frac{\delta(\rho')}{2\pi\rho'} \tag{S16}$$

Note that the wave equation is written in the cylindrical coordinate system. For $\rho' \neq 0$, the above equation becomes

$$\left[\frac{1}{\rho'}\frac{d}{d\rho'}\left(\rho'\frac{d}{d\rho'}\right) + k_{\rho'}'\right]g'(\rho') = 0 \tag{S17}$$

where

$$k_{\rho'}' = \sqrt{k'^2 - {k_{z'}'}^2} = \sqrt{k'^2 - \frac{\omega'^2}{v_e'^2}} = \frac{\omega'}{c}n\sqrt{1 - \frac{c^2}{n^2 v_e'^2}} \tag{S18}$$

Note that $k_{z'}' = -\omega'/v_e'$. The equation (S17) is the standard zeroth-order Bessel equation. Since equation (S17) exhibits a singularity at $\rho' = 0$ and the solution to the equation should represent an outgoing wave due to causality, we choose

$$g'(\rho') = CH_0^{(1)}\left(k_{\rho'}'\rho'\right) \tag{S19}$$

The constant C can be determined by matching the boundary condition at $\rho' \to 0$. Integrating equation (S16) over an infinitesimal area $2\pi\rho' d\rho'$ and letting $\rho' \to 0$, we have

$$\lim_{\rho' \to 0} 2\pi\rho'\frac{dg'(\rho')}{d\rho'} = -1 \tag{S20}$$

Using the asymptotic formula for $H_0^{(1)}\left(k_{\rho'}'\rho'\right) \approx i(2/\pi)\ln\left(k_{\rho'}'\rho'\right)$ when $\rho' \to 0$, we obtain $C = i/4$ and thus

$$g'(\rho') = \frac{i}{4}H_0^{(1)}\left(k_{\rho'}'\rho'\right) \tag{S21}$$

Substituting equation (S21) into equation (S15) and equation (S13), we obtain

$$\bar{E}'(\bar{r}', \omega') = -\frac{q}{8\pi\omega'\varepsilon_0\varepsilon_r}\left[\hat{z}'k'^2 - i\frac{\omega'}{v_e'}\nabla'\right]H_0^{(1)}\left(k_{\rho'}'\rho'\right)e^{-i\omega' z'/v_e'} \tag{S22}$$

The z' axis and ρ' axis components of the electric field can be further expressed as

$$E'_{z'}(\bar{r}',\omega') = -\frac{q}{8\pi\omega'\varepsilon_0\varepsilon_r} {k'_{\rho'}}^2 H_0^{(1)}\left(k'_{\rho'}\rho'\right) e^{-i\omega' z\,/v'_{\mathrm{e}}} \tag{S23}$$

$$E'_{\rho'}(\bar{r}',\omega') = \frac{q}{8\pi\omega'\varepsilon_0\varepsilon_r}\left(-i\frac{\omega'}{v'_{\mathrm{e}}}\right) k'_{\rho'} H_1^{(1)}\left(k'_{\rho'}\rho'\right) e^{-i\omega' z'/v'_{\mathrm{e}}} \tag{S24}$$

The magnetic field can be further calculated using equation (S1) as

$$H'_{\phi'}(\bar{r},\omega) = \frac{iq}{8\pi} k'_{\rho'} H_1^{(1)}\left(k'_{\rho'}\rho'\right) e^{-i\omega' z'/v'_{\mathrm{e}}} \tag{S25}$$

Thus, the time-domain values of electromagnetic field under the medium co-moving frame S' can be expressed as

$$E'_{z'}(\bar{r}',t') = \int d\omega' \frac{-q}{8\pi\omega'\varepsilon_0\varepsilon_r} {k'_{\rho'}}^2 H_0^{(1)}\left(k'_{\rho'}\rho'\right) e^{i(-\omega' z'/v'_{\mathrm{e}} - \omega' t')} \tag{S26}$$

$$E'_{\rho'}(\bar{r}',t') = \int d\omega' \frac{q}{8\pi\omega'\varepsilon_0\varepsilon_r}\left(-i\frac{\omega'}{v'_{\mathrm{e}}}\right) k'_{\rho'} H_1^{(1)}\left(k'_{\rho'}\rho'\right) e^{i(-\omega' z'/v'_{\mathrm{e}} - \omega' t')} \tag{S27}$$

$$H'_{\phi'}(\bar{r}',t') = \int d\omega' \frac{iq}{8\pi} k'_{\rho'} H_1^{(1)}\left(k'_{\rho'}\rho'\right) e^{i(-\omega' z'/v'_{\mathrm{e}} - \omega' t')} \tag{S28}$$

Section S2: Cherenkov radiation under the static laboratory frame *S*

In this section, we will solve for the field distribution under the static laboratory frame S, which corresponds to a moving isotropic nondispersive medium. The notation and schematic are consistent with Fig. 1(d) in the main text. Since the moving isotropic medium is equivalent to a bi-anisotropic medium [42], direct calculation of the field distribution becomes challenging. Therefore, we use Lorentz transformation to solve for the field distribution under the frame S. When the medium moves with a velocity of $\bar{v}_{\mathrm{medium}} = \hat{z} v_{\mathrm{medium}}$, the Lorentz transformation of space and time from frame S' to S can be expressed as

$$\rho = \rho' \tag{S29}$$

$$\phi = \phi' \tag{S30}$$

$$z = \gamma(z' + v_{\mathrm{medium}} t') \tag{S31}$$

$$ct = \gamma\left(ct' + \frac{v_{\mathrm{medium}}}{c} z'\right) \tag{S32}$$

where $\gamma = \frac{1}{\sqrt{1 - v_{\mathrm{medium}}^2/c^2}}$ is the Lorentz factor. For further convenience, we also write down the spacetime transformation from frame S' to S as

$$\rho' = \rho \tag{S33}$$

$$\phi' = \phi \tag{S34}$$

$$z' = \gamma(z - v_{\mathrm{medium}} t) \tag{S35}$$

$$ct' = \gamma\left(ct - \frac{v_{\mathrm{medium}}}{c} z\right) \tag{S36}$$

Before we transform the field distribution, we first transform the frequency ω' and the wavevector $\bar{k}'$ from frame S' to S as

$$k_\rho = k'_{\rho'} \tag{S37}$$

$$k_z = \gamma k'_{z'} + \gamma v_{\mathrm{medium}} \frac{\omega'}{c^2} = \omega' \gamma \left(\frac{v_{\mathrm{medium}}}{c^2} - \frac{1}{v'_{\mathrm{e}}}\right) \tag{S38}$$

$$\omega = \gamma\left(\omega' + v_{\mathrm{medium}} k'_{z'}\right) = \omega' \gamma \left(1 - \frac{v_{\mathrm{medium}}}{v'_{\mathrm{e}}}\right) \tag{S39}$$

By dividing equation (S39) by equation (S38), we find that

$$k_z = -\frac{\omega}{v_{\mathrm{e}}} \tag{S40}$$

where $v_{\mathrm{e}} = \frac{v'_{\mathrm{e}} - v_{\mathrm{medium}}}{1 - v'_{\mathrm{e}} v_{\mathrm{medium}}/c^2}$. Thus, due to the invariant property of the phase of the field distribution, the $e^{i(-\omega' z'/v'_{\mathrm{e}} - \omega' t')}$ of equations (S26)-(S28) can be transformed to $e^{i(-\omega\ /v_{\mathrm{e}} - \omega t)}$. Meanwhile, the ω' and $k'_{\rho'}$ in equations (S26)-(S28) can be transformed as

$$\omega' = \gamma(\omega - v_{\mathrm{medium}} k_z) = \omega \gamma \left(1 + \frac{v_{\mathrm{medium}}}{v_{\mathrm{e}}}\right) \tag{S41}$$

$$k'_{\rho'} = k_\rho = \frac{\omega \gamma (1 + v_{\mathrm{medium}}/v_{\mathrm{e}})}{c} n \sqrt{1 - \frac{c^2}{n^2 {v'_{\mathrm{e}}}^2}} \tag{S42}$$

Decomposing the field vectors into components parallel and perpendicular to the medium velocity $\bar{v}_{\mathrm{medium}}$, the Lorentz transformation of the field distribution follows the following rule

$$\bar{E}_\parallel(\bar{r}, t) = \bar{E}'_\parallel(\bar{r}', t') \tag{S43}$$

$$\bar{E}_\perp(\bar{r}, t) = \gamma \left(\bar{E}'_\perp(\bar{r}', t') - \frac{v_{\mathrm{medium}}}{c} \hat{z} \times c\bar{B}'_\perp(\bar{r}', t')\right) \tag{S44}$$

$$\bar{H}_\perp(\bar{r}, t) = \gamma \left(\bar{H}'_\perp(\bar{r}', t') + \frac{v_{\mathrm{medium}}}{c} \hat{z} \times c\bar{D}'_\perp(\bar{r}', t')\right) \tag{S45}$$

Equations (S43)-(S45) can be further rewritten as

$$E_z(\bar{r},t) = E'_{z'}(\bar{r}',t') \tag{S46}$$

$$E_\rho(\bar{r},t) = \gamma\left(E'_{\rho'}(\bar{r}',t') + v_{\text{medium}}\mu_0\mu_r H'_{\phi'}(\bar{r}',t')\right) \tag{S47}$$

$$H_\phi(\bar{r},t) = \gamma\left(H'_{\phi'}(\bar{r}',t') + v_{\text{medium}}\varepsilon_0\varepsilon_r E'_{\rho'}(\bar{r}',t')\right) \tag{S48}$$

Substituting equations (S26)-(S28), (S33)-(S36) and (S41)-(S42) into equations (S46)-(S48), the field distribution under the frame S can be obtained after some calculations as

$$E_z(\bar{r},t) = \int d\omega \frac{-q}{8\pi\omega\varepsilon_0\varepsilon_r} k_\rho^2 H_0^{(1)}(k_\rho\rho) e^{i(-\omega z/v_{\text{e}}-\omega\ )} \tag{S49}$$

$$E_\rho(\bar{r},t) = \int d\omega\gamma^2 \frac{-iq}{8\pi\varepsilon_0\varepsilon_r v_{\text{e}}}\left(1+\frac{v_{\text{e}}v_{\text{medium}}}{c^2}\right)\left(1-\frac{v_{\text{medium}}v'_{\text{e}}}{c^2}n^2\right) k_\rho H_1^{(1)}(k_\rho\rho) e^{i(-\omega z/v_{\text{e}}-\omega t)} \tag{S50}$$

$$H_\phi(\bar{r},t) = \int d\omega \frac{iq}{8\pi} k_\rho H_1^{(1)}(k_\rho\rho) e^{i(-\omega\ /v_{\text{e}}-\omega t)} \tag{S51}$$

In order to demonstrate the time-domain field distribution by finite integration, we treat the current density and charge density under the laboratory frame S having a Gaussian-shape spatial dependence as

$$J_z(\bar{r},t) = -qv_{\text{e}}\delta(z+v_{\text{e}}t)\frac{\delta(\rho)}{2\pi\rho}\frac{1}{\sigma_z\sqrt{2\pi}} e^{-\frac{(z+v_{\text{e}}t)^2}{2\sigma_z^2}} \tag{S52}$$

$$\rho(\bar{r},t) = q\delta(z+v_{\text{e}}t)\frac{\delta(\rho)}{2\pi\rho}\frac{1}{\sigma_z\sqrt{2\pi}} e^{-\frac{(z+v_{\text{e}}t)^2}{2\sigma_z^2}} \tag{S53}$$

The Lorentz transformation of current density from frame S to S' can be expressed as

$$J'_{z'}(\bar{r}',t') = \gamma J_z(\bar{r},t) - \gamma v_{\text{medium}}\rho(\bar{r},t) \tag{S54}$$

By substituting equations (S52)-(S53) into equation (S54), we can obtain the current density under the co-moving frame S' as

$$J'_{z'}(\bar{r}',t') = -qv'_{\text{e}}\delta(z'+v'_{\text{e}}t')\frac{\delta(\rho')}{2\pi\rho'}\frac{1}{\sigma_z\sqrt{2\pi}} e^{-\frac{(z'+v'_{\text{e}}t')^2}{2\sigma_z'^2}} \tag{S55}$$

where $\sigma'_z = \frac{\sigma_z}{\gamma\left(1+\frac{v_{\text{e}}v_{\text{medium}}}{c^2}\right)}$. Follow the same strategy, we can obtain the field distribution under frame S as

$$E_z(\bar{r},t) = \int d\omega \frac{\sigma'_z}{\sigma_z}\frac{-q}{8\pi\omega\varepsilon_0\varepsilon_r} k_\rho^2 H_0^{(1)}(k_\rho\rho) e^{i(-\omega z/v_{\text{e}}-\omega t)} e^{-\frac{\sigma_z^2\omega^2}{2\,v_{\text{e}}^2}} \tag{S56}$$

$$E_\rho(\bar{r},t) = \int d\omega \frac{\sigma'_z}{\sigma_z}\gamma^2 \frac{-iq}{8\pi\varepsilon_0\varepsilon_r v_{\text{e}}}\left(1+\frac{v_{\text{e}}v_{\text{medium}}}{c^2}\right)\left(1-\frac{v_{\text{medium}}v'_{\text{e}}}{c^2}n^2\right) k_\rho H_1^{(1)}(k_\rho\rho) e^{i(-\omega z/v_{\text{e}}-\omega t)} e^{-\frac{\sigma_z^2\omega^2}{2\,v_{\text{e}}^2}} \tag{S57}$$

$$H_\phi(\bar{r},t) = \int d\omega \frac{\sigma'_z}{\sigma_z}\frac{iq}{8\pi} k_\rho H_1^{(1)}(k_\rho\rho) e^{i(-\omega z/v_{\text{e}}-\omega t)}\, e^{-\frac{\sigma_z^2\omega^2}{2\,v_{\text{e}}^2}} \tag{S58}$$

The Fig. 2(c) in the main text is drawn using equation (S56) with $\sigma_z = 6\mu\text{m}$ and integrating from -50 THz to 50 THz.

Section S3: Dispersion relation for moving isotropic nondispersive media

In this section, we will derive the dispersion relation for the moving isotropic medium under the laboratory frame S using the kDB system [42] and use the isofrequency contours to analyze the directions of the group velocities for specific eigenmodes. Generally, isotropic media in motion exhibit response tensors with the same structure as that of stationary bianisotropic media [42], while their analytic properties differ [113-118]. The bianisotropy inherent to moving media could be essentially characterized by the cross-coupling between the electric and magnetic fields represented by cross-coupling tensors $\bar{\bar{\xi}}$ and $\bar{\bar{\zeta}}$, apart from common permittivity and permeability tensors $\bar{\bar{\varepsilon}}$ and $\bar{\bar{\mu}}$. Specifically, when isotropic media with permittivity ε and permeability μ move with a velocity $\bar{v}_{\text{medium}} = \hat{z}v_{\text{medium}}$, the constitution relation of the resulting bianisotropic medium is given by

$$\bar{D} = \bar{\bar{\varepsilon}} \cdot \bar{E} + \bar{\bar{\xi}} \cdot \bar{H} \tag{S59}$$

$$\bar{B} = \bar{\bar{\zeta}} \cdot \bar{E} + \bar{\bar{\mu}} \cdot \bar{H} \tag{S60}$$

$$\bar{\bar{\varepsilon}} = \begin{bmatrix} \frac{\varepsilon\left(1 - v_{\text{medium}}^2/c^2\right)}{1 - \varepsilon\mu v_{\text{medium}}^2} & 0 & 0 \\ 0 & \frac{\varepsilon\left(1 - v_{\text{medium}}^2/c^2\right)}{1 - \varepsilon\mu v_{\text{medium}}^2} & 0 \\ 0 & 0 & \varepsilon \end{bmatrix}, \ \bar{\bar{\mu}} = \begin{bmatrix} \frac{\mu\left(1 - v_{\text{medium}}^2/c^2\right)}{1 - \varepsilon\mu v_{\text{medium}}^2} & 0 & 0 \\ 0 & \frac{\mu\left(1 - v_{\text{medium}}^2/c^2\right)}{1 - \varepsilon\mu v_{\text{medium}}^2} & 0 \\ 0 & 0 & \mu \end{bmatrix} \tag{S61}$$

$$\bar{\bar{\xi}} = \begin{bmatrix} 0 & -\frac{v_{\text{medium}}\left(c^2\varepsilon\mu - 1\right)}{c^2\left(1 - \varepsilon\mu v_{\text{medium}}^2\right)} & 0 \\ \frac{v_{\text{medium}}\left(c^2\varepsilon\mu - 1\right)}{c^2\left(1 - \varepsilon\mu v_{\text{medium}}^2\right)} & 0 & 0 \\ 0 & 0 & 0 \end{bmatrix}, \bar{\bar{\zeta}} = \begin{bmatrix} 0 & \frac{v_{\text{medium}}\left(c^2\varepsilon\mu - 1\right)}{c^2\left(1 - \varepsilon\mu v_{\text{medium}}^2\right)} & 0 \\ -\frac{v_{\text{medium}}\left(c^2\varepsilon\mu - 1\right)}{c^2\left(1 - \varepsilon\mu v_{\text{medium}}^2\right)} & 0 & 0 \\ 0 & 0 & 0 \end{bmatrix} \tag{S62}$$

where c is the light speed in vacuum. As a result from equations (S59)-(S62), the isofrequency contours could manifest themselves as a hyperbolic or elliptical shape [42].

To further obtain the dispersion relation in a more convenient way under the kDB system [42], the so-called $\bar{E}\bar{H}$ representation of constitution relation in equations (S59)-(S62) could be equivalently transformed to $\bar{D}\bar{B}$ representation as follows

$$\bar{E} = \bar{\bar{\kappa}} \cdot \bar{D} + \bar{\bar{\chi}} \cdot \bar{B} \tag{S63}$$

$$\bar{H} = \bar{\bar{\gamma}} \cdot \bar{D} + \bar{\bar{\nu}} \cdot \bar{B} \tag{S64}$$

The constitutive tensors in equations (S63)-(S64) can be expressed as

$$\bar{\bar{\kappa}} = \begin{bmatrix} \kappa & 0 & 0 \\ 0 & \kappa & 0 \\ 0 & 0 & \kappa_z \end{bmatrix} \tag{S65}$$

$$\bar{\bar{\nu}} = \begin{bmatrix} \nu & 0 & 0 \\ 0 & \nu & 0 \\ 0 & 0 & \nu_z \end{bmatrix} \tag{S66}$$

$$\bar{\bar{\chi}} = \bar{\bar{\gamma}}^{+} = \begin{bmatrix} 0 & \chi & 0 \\ -\chi & 0 & 0 \\ 0 & 0 & 0 \end{bmatrix} \tag{S67}$$

where $\kappa = \frac{c^2\mu(1-v_{\text{medium}}^2/c^2)}{n^2-v_{\text{medium}}^2/c^2}$, $\kappa_z = 1/\varepsilon$, $\nu = \frac{c^2\varepsilon(1-v_{\text{medium}}^2/c^2)}{n^2-v_{\text{medium}}^2/c^2}$, $\nu_z = 1/\mu$ and $\chi = \frac{v_{\text{medium}}(n^2-1)}{n^2-v_{\text{medium}}^2/c^2}$ are the corresponding constitutive parameters. In order to generate dispersion relation from the constitutive relations, we transform the constitutive relations equations (S65)-(S67) from xyz system to kDB system. The kDB system consists of three unit vectors $\hat{e}_1$, $\hat{e}_2$ and $\hat{e}_3$. The unit vector $\hat{e}_3$ is in the direction of the wavevector $\bar{k}$ such that $\bar{k} = \hat{e}_3 k$, which is also in the $\hat{r}$ direction under spherical coordinate. The unit vectors $\hat{e}_2$ and $\hat{e}_1$ are in the direction of $\hat{\theta}$ and $-\hat{\phi}$, respectively. Thus, the unit vectors $\hat{e}_2$ and $\hat{e}_1$ form the DB plane since the field vectors $\bar{D}$ and $\bar{B}$ are always perpendicular to the wavevector $\bar{k}$. For an arbitrary vector $\bar{A}$ in xyz coordinate system, its corresponding vector $\bar{A}_k$ can be obtained as

$$\bar{A}_k = \bar{\bar{T}} \cdot \bar{A} = \begin{bmatrix} \sin\phi & -\cos\phi & 0 \\ \cos\theta\cos\phi & \cos\theta\sin\phi & -\sin\theta \\ \sin\theta\cos\phi & \sin\theta\sin\phi & \cos\theta \end{bmatrix} \cdot \bar{A} \tag{S68}$$

The inverse of $\bar{\bar{T}}$ can be simply calculated as

$$\bar{\bar{T}}^{-1} = \begin{bmatrix} \sin\phi & \cos\theta\cos\phi & \sin\theta\cos\phi \\ -\cos\phi & \cos\theta\sin\phi & \sin\theta\sin\phi \\ 0 & -\sin\theta & \cos\theta \end{bmatrix} \tag{S69}$$

The constitutive relations in xyz system can be transformed to kDB system as

$$\bar{E}_k = \bar{\bar{\kappa}}_k \cdot \bar{D}_k + \bar{\bar{\chi}}_k \cdot \bar{B}_k \tag{S70}$$

$$\bar{H}_k = \bar{\bar{\gamma}}_k \cdot \bar{D}_k + \bar{\bar{\nu}}_k \cdot \bar{B}_k \tag{S71}$$

where

$$\bar{\bar{\kappa}}_k = \bar{\bar{T}} \cdot \bar{\bar{\kappa}} \cdot \bar{\bar{T}}^{-1} \tag{S72}$$

$$\bar{\bar{\chi}}_k = \bar{\bar{T}} \cdot \bar{\bar{\chi}} \cdot \bar{\bar{T}}^{-1} \tag{S73}$$

$$\bar{\bar{\gamma}}_k = \bar{\bar{T}} \cdot \bar{\bar{\gamma}} \cdot \bar{\bar{T}}^{-1} \tag{S74}$$

$$\bar{\bar{\nu}}_k = \bar{\bar{T}} \cdot \bar{\bar{\nu}} \cdot \bar{\bar{T}}^{-1} \tag{S75}$$

Substituting equations (S65)-(S69) into equations (S72)-(S75), we can obtain the constitutive tensors under kDB system as

$$\bar{\bar{\kappa}}_k = \begin{bmatrix} \kappa & 0 & 0 \\ 0 & \kappa\cos^2\theta + \kappa_z \sin^2\theta & (\kappa - \kappa_z)\sin\theta\cos\theta \\ 0 & (\kappa - \kappa_z)\sin\theta\cos\theta & \kappa\sin^2\theta + \kappa_z\cos^2\theta \end{bmatrix} \tag{S76}$$

$$\bar{\bar{\nu}}_k = \begin{bmatrix} \nu & 0 & 0 \\ 0 & \nu\cos^2\theta + \nu_z \sin^2\theta & (\nu - \nu_z)\sin\theta\cos\theta \\ 0 & (\nu - \nu_z)\sin\theta\cos\theta & \nu\sin^2\theta + \nu_z\cos^2\theta \end{bmatrix} \tag{S77}$$

$$\bar{\bar{\chi}}_k = \bar{\bar{\gamma}}_k^{+} = \begin{bmatrix} 0 & \chi\cos\theta & \chi\sin\theta \\ -\chi\cos\theta & 0 & 0 \\ -\chi\sin\theta & 0 & 0 \end{bmatrix} \tag{S78}$$

Substituting equations (S70)-(S71) and equations (S76)-(S78) to Maxwell equations $\bar{k} \times \bar{E}_k = \omega \bar{B}_k$, $\bar{k} \times \bar{H}_k = -\omega \bar{D}_k$ and using the condition of $\bar{k} = \hat{e}_3 k$ under kDB system, we obtain

$$\begin{bmatrix} \kappa_{11} & \kappa_{12} \\ \kappa_{21} & \kappa_{22} \end{bmatrix} \begin{bmatrix} D_1 \\ D_2 \end{bmatrix} = -\begin{bmatrix} \chi_{11} & \chi_{12} - u \\ \chi_{21} + u & \chi_{22} \end{bmatrix} \begin{bmatrix} B_1 \\ B_2 \end{bmatrix} \tag{S79}$$

$$\begin{bmatrix} \nu_{11} & \nu_{12} \\ \nu_{21} & \nu_{22} \end{bmatrix} \begin{bmatrix} B_1 \\ B_2 \end{bmatrix} = -\begin{bmatrix} \gamma_{11} & \gamma_{12} + u \\ \gamma_{21} - u & \gamma_{22} \end{bmatrix} \begin{bmatrix} D_1 \\ D_2 \end{bmatrix} \tag{S80}$$

where $u = \omega/k$. Note that $B_3 = D_3 = 0$ since $\bar{k} \cdot \bar{B}_k = 0$ and $\bar{k} \cdot \bar{D}_k = 0$. By eliminating $\bar{B}$, we can obtain the following equation for $\bar{D}$ as

$$\begin{bmatrix} 1 - (u - \chi\cos\theta)^2/[\kappa(\nu\cos^2\theta + \nu_z\sin^2\theta)] & 0 \\ 0 & 1 - (u - \chi\cos\theta)^2/[\nu(\kappa\cos^2\theta + \kappa_z\sin^2\theta)] \end{bmatrix} \begin{bmatrix} D_1 \\ D_2 \end{bmatrix} = 0 \tag{S81}$$

As can been seen from equation (S81), there are two cases of nontrivial solutions. For $D_1 \neq 0$ and $D_2 = 0$, we have $1-(u-\chi\cos\theta)^2/[\kappa(\nu\cos^2\theta+\nu_z\sin^2\theta)]=0$. For $D_1 = 0$ and $D_2 \neq 0$, we have $1-(u-\chi\cos\theta)^2/[\nu(\kappa\cos^2\theta+\kappa_z\sin^2\theta)]=0$. However, since $\kappa\nu_z=\kappa_z\nu=\frac{c^2(1-v_{\text{medium}}^2/c^2)}{n^2-v_{\text{medium}}^2/c^2}$, these two cases are degenerate and share the same condition. Substituting $k_z^2=k^2\cos^2\theta$ and $k_x^2+k_y^2=k^2\sin^2\theta$ into this condition, we obtain the dispersion relation as

$$k_x^2+k_y^2+\frac{c^2-n^2v_{\text{medium}}^2}{c^2-v_{\text{medium}}^2}\left[k_z-\frac{nc+v_{\text{medium}}}{nv_{\text{medium}}+c}\frac{\omega}{c}\right]\cdot\left[k_z-\frac{nc-v_{\text{medium}}}{nv_{\text{medium}}-c}\frac{\omega}{c}\right]=0 \quad \text{(S82)}$$

Without loss of generality, for the eigenmodes with $\bar{k}=\hat{x}k_x+\hat{z}k_z$ ($k_y=0$), we have

$$k_x^2+\frac{c^2-n^2v_{\text{medium}}^2}{c^2-v_{\text{medium}}^2}\left[k_z-\frac{nc+v_{\text{medi}}}{nv_{\text{medium}}+c}\frac{\omega}{c}\right]\cdot\left[k_z-\frac{nc-v_{\text{medium}}}{nv_{\text{medium}}-c}\frac{\omega}{c}\right]=0 \quad \text{(S83)}$$

In order to analyze the directions of the group velocities $\bar{v}_{\text{g}}$ for eigenmodes with specific wavevectors $\bar{k}$, we draw the isofrequency contours with $v_{\text{medium}}/c=0.45$ and $v_{\text{medium}}/c=0.75$ in Fig. S2, which correspond to subluminal scenario and superluminal scenario, respectively. For conceptual illustration, below $n=2$ is used. The dashed curves correspond to the same v_{medium} at a slightly higher frequency. The directions of the group velocities for specific wavevectors should originate from the solid curves towards the dashed curves.

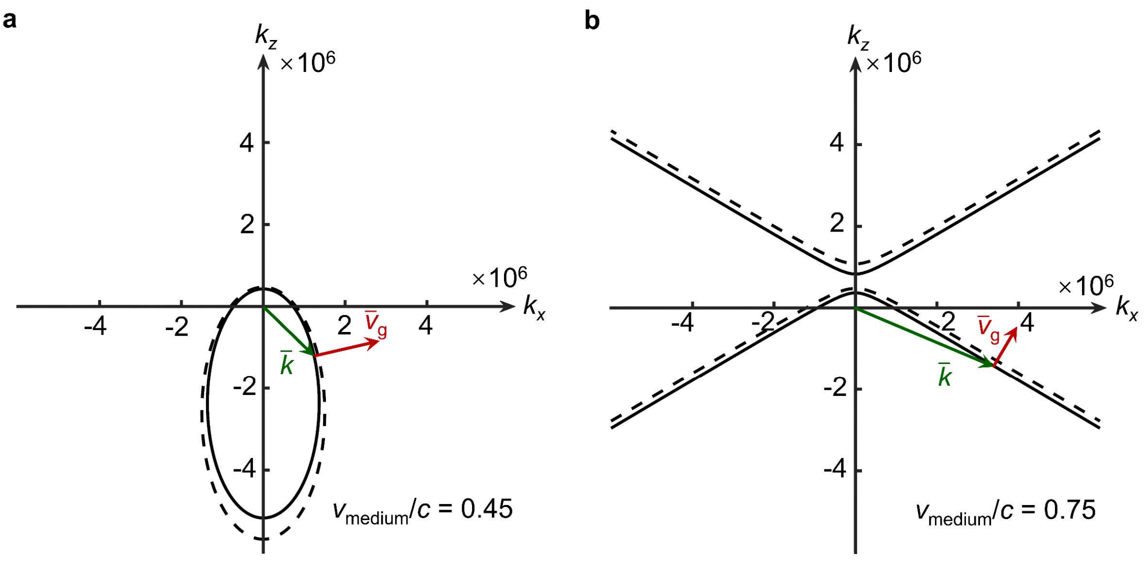

FIG. S2. Directions of the group velocities for specific wavevectors. Here and below, we set the refractive index $n=2$ for illustration. (a) and (b) are isofrequency contours correspond to $v_{\text{medium}}/c=0.45$ and $v_{\text{medium}}/c=$

0.75, which correspond to subluminal scenario and superluminal scenario, respectively. The dashed curves correspond to the same medium at a slightly higher frequency.

Section S4: Derivation of the radiation angle θ under the static laboratory frame S

In this section, we derive the radiation angle θ under the static laboratory frame S through equation (S83). The radiation angle θ under the frame S, which is the angle between $\bar{v}_{\mathrm{g}}$ and the moving direction of electron $\bar{v}_{\mathrm{e}}$ (or $-\hat{z}$), and can be easily defined as

$$\theta = \arccos\left(-\frac{v_{\mathrm{g},z}}{\sqrt{v_{\mathrm{g},z}^2 + v_{\mathrm{g},\rho}^2}}\right) \tag{S84}$$

Since $v_{\mathrm{g}} = \frac{\partial \omega}{\partial k}$, the $\hat{\rho}$ ($\hat{z}$) component of $\bar{v}_{\mathrm{g}}$ can be easily calculated through equation (S83) as

$$v_{\mathrm{g},\rho} = \frac{\partial \omega}{\partial k_\rho} = \frac{-k_\rho\left(1 - v_{\mathrm{medium}}^2/c^2\right)}{\left(n^2 v_{\mathrm{medium}} - v_{\mathrm{medium}}\right)\frac{k_z}{c^2} - \left(n^2 - v_{\mathrm{medium}}^2/c^2\right)\frac{\omega}{c^2}} \tag{S85}$$

$$v_{\mathrm{g},z} = \frac{\partial \omega}{\partial k_z} = \frac{k_z\left(n^2 v_{\mathrm{medium}}^2/c^2 - 1\right) - \left(n^2 v_{\mathrm{medium}} - v_{\mathrm{medium}}\right)\frac{\omega}{c^2}}{\left(n^2 v_{\mathrm{medium}} - v_{\mathrm{medium}}\right)\frac{k_z}{c^2} - \left(n^2 - v_{\mathrm{medium}}^2/c^2\right)\frac{\omega}{c^2}} \tag{S86}$$

where $k_\rho = \frac{\omega\gamma(1 + v_{\mathrm{medium}}/v_{\mathrm{e}})}{c} n\sqrt{1 - \frac{c^2}{n^2 v_{\mathrm{e}}'^2}}$ and $k_z = -\omega/v_{\mathrm{e}}$ are components of corresponding wavevector and $\gamma = \frac{1}{\sqrt{1 - v_{\mathrm{medium}}^2/c^2}}$ is the Lorentz factor.

Section S5: More discussion on reversed Cherenkov radiation via Fizeau-Fresnel drag

S5.1 Influence of the moving-medium velocity on the symmetry center and shape of the isofrequency contour

In this subsection, we show the influence of the moving-medium velocity on the symmetry center and shape of the isofrequency contour. The medium velocity v_{medium} is a key parameter to determine both the symmetry center and the shape of the isofrequency contour. On the one hand, we show in Fig. S3(a) that the position of symmetry center along the k_z direction of the isofrequency contour, namely $k_{z,\mathrm{symmetry}}(\omega, v_{\mathrm{medi}}\ \ ) = \frac{\omega}{c} \cdot \frac{(n^2 - 1) v_{\mathrm{medium}}/c}{n^2 v_{\mathrm{medium}}^2/c^2 - 1}$, is a function of both the frequency ω and the medium velocity v_{medium}, where n is the refractive index under the medium co-moving frame. On the other hand, by increasing the medium velocity, we show the explicit topological transition of the isofrequency contours in Figs. S3(b) and S3(c), whose shape evolves from a circle to a set of ellipses in the subluminal scenario in Fig. S3(b), and to a set of hyperbolas in the superluminal scenario in Fig. S3(c).

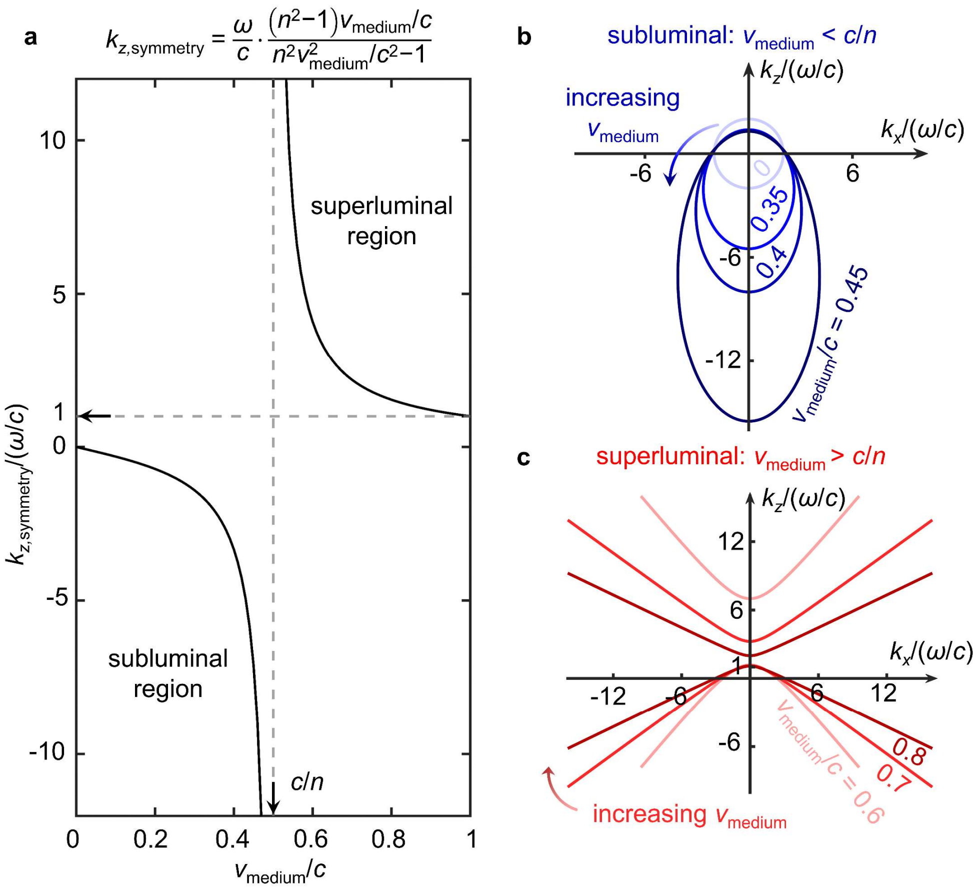

FIG. S3. Influence of the moving-medium velocity on the symmetry center and shape of the isofrequency contour. For illustration here, the refractive index $n = 2$. (a) Dependence of the symmetry center of the isofrequency contour on the medium velocity. (b) and (c) Isofrequency contours of the moving media with various medium velocities. As the medium velocity increases in (a), the position of the symmetry center $k_{z,\text{symmetry}}$ along the k_z direction moves from 0 towards $-\infty$ in the subluminal case and from $+\infty$ towards ω/c in the superluminal case. For the subluminal scenario in (b), the isofrequency contours evolves from a circle at $v_{\text{medium}} = 0$ to a set of ellipses for $v_{\text{medium}} < c/n$. For the superluminal case with $v_{\text{medium}} > c/n$ in (c), the isofrequency contours are a set of hyperbolas.

S5.2 Influence of nonparallel directions between the particle and medium velocities on reversed Cherenkov radiation via Fizeau-Fresnel drag

In this subsection, we discuss the influence of nonparallel directions between the particle and medium velocities on reversed Cherenkov radiation via Fizeau-Fresnel drag. Intriguingly, nonparallel moving directions between the particle velocity and the medium velocity could result to asymmetric excitation of eigenmodes of light and the simultaneous emergence of reversed and conventional Cherenkov radiations. In Figs. S4(a) and S4(b), we conceptually show the asymmetric excitation of Cherenkov eigenmodes via the intersections between the nonparallel particle dispersion line and the isofrequency contour of moving media. We further highlight in Fig. S4(c) the simultaneous emergence of reversed and conventional Cherenkov radiations, by showing the dependence of Cherenkov radiation angles on nonparallel particle velocities.

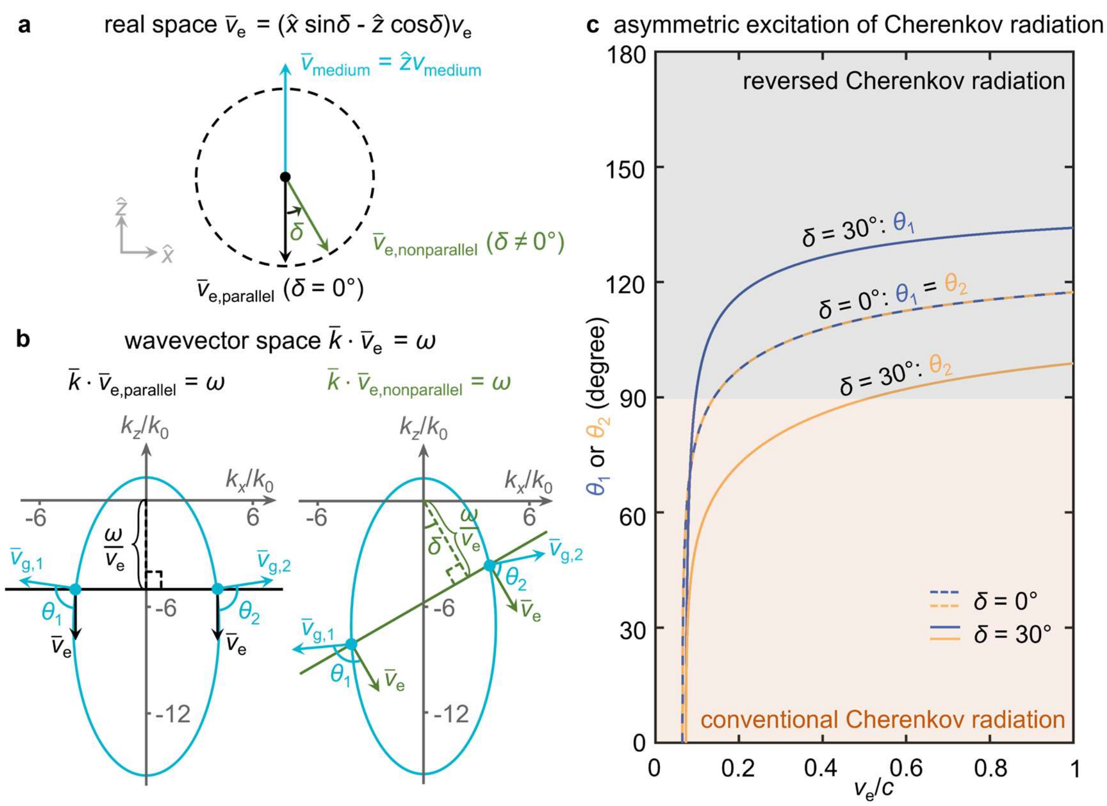

FIG. S4. Influence of nonparallel directions between the particle and medium velocities on reversed Cherenkov radiation via Fizeau-Fresnel drag. Here we use $v_e/c = 0.2$ in (b) and $v_{medium}/c = 0.45$. (a) and (b) Conceptual illustration of Cherenkov radiation from the charged particle with nonparallel velocity to the moving medium. (c) Dependence of the Cherenkov angles on the particle velocity under nonparallel and parallel cases. Without loss of generality in (a), we use the particle velocity $\bar{v}_e = (\hat{x}\sin\delta - \hat{z}\cos\delta)v_e$ under both parallel ($\delta = 0°$) and nonparallel ($\delta \neq 0°$) particle velocities. In (b), the particle dispersion line is governed by $\bar{k} \cdot \bar{v}_e = \omega$, whose intersections with the isofrequency contour indicate the excitation of Cherenkov eigenmodes. The corresponding Cherenkov angles between the particle velocity and group velocities of these eigenmodes are denoted by θ_1 and θ_2. As a result in (c), while $\theta_1 = \theta_2$ in the conventionally parallel case of $\delta = 0°$, nonparallel directions between the particle and medium velocities (e.g., $\delta = 30°$) yields asymmetric excitation of Cherenkov eigenmodes with $\theta_1 \neq \theta_2$. Upon close inspection, this asymmetric excitation could enable the simultaneous emergence of reversed and conventional Cherenkov radiations with $\theta_1 > 90°$ and $\theta_2 < 90°$ at certain particle velocities (e.g., $0.2c < v_e < 0.4c$).

S5.3 Geometric explanation of the moving-medium velocity threshold for reversed Cherenkov radiation via Fizeau-Fresnel drag

In this subsection, we provide a geometric explanation of the moving-medium velocity threshold for reversed Cherenkov radiation via Fizeau-Fresnel drag. The underlying mechanism of our revealed reversed Cherenkov radiation is that the moving media drag the emitted light towards the reversed direction of moving charged particles. As such, the medium velocity threshold for reversed Cherenkov radiation is quantitatively related to the minimum group velocity component along the direction of the particle motion under the medium co-moving frame S', namely $v_{\mathrm{th,rCR,medium}} = \min\left|v'_{g,z}\right|$. On this basis, we show in Fig. S5 that the scaling factor of $1/n^2$ can be simply constructed via the geometric relation between the particle velocity and the group velocity of light.

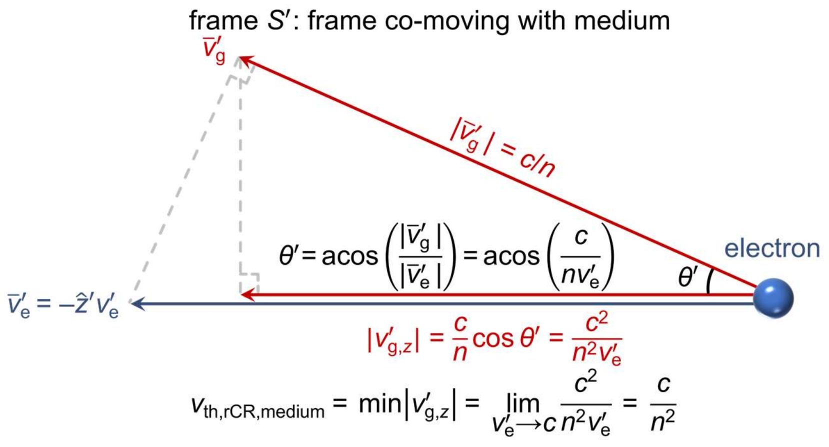

FIG. S5. Geometric explanation of the moving-medium velocity threshold for reversed Cherenkov radiation via Fizeau-Fresnel drag. The origin of scaling factor of $1/n^2$ lies in the z-component of the group velocity of light.

<u>S5.4 Influence of the frequency dispersion and material loss on reversed Cherenkov radiation via Fizeau-Fresnel drag</u>

In this subsection, we discuss the influence of frequency dispersion and material loss on reversed Cherenkov radiation via Fizeau-Fresnel drag. In principle, our revealed reversed Cherenkov radiation could remain valid in media with reasonable dispersion and losses. The underlying reason is that the frequency dispersion and the moderate material loss do not fundamentally alter the direction of the group velocity of the reversed Cherenkov radiation, although they can modify its magnitude to some extent.

Specifically, below we derive the general expressions for the direction and magnitude of the group velocity:

$$\theta_{\mathrm{rCR}} = \mathrm{Re}\left\{\arctan\left(-\frac{v_{\mathrm{g},\rho}}{v_{\mathrm{g},z}}\right)\right\} = \mathrm{Re}\left\{\arctan\left(\frac{k_\rho\left(1 - v_{\mathrm{medium}}^2/c^2\right)}{k_z\left(\varepsilon(\omega')v_{\mathrm{medium}}^2/c^2 - 1\right) - \left(\varepsilon(\omega')v_{\mathrm{medium}} - v_{\mathrm{medium}}\right)\frac{\omega}{c^2}}\right)\right\} \tag{S87}$$

$$v_{\mathrm{g},z} = \frac{k_z\left(\varepsilon(\omega')v_{\mathrm{medium}}^2/c^2 - 1\right) - \left(\varepsilon(\omega')v_{\mathrm{medium}} - v_{\mathrm{medium}}\right)\frac{\omega}{c^2}}{\left(\varepsilon(\omega')v_{\mathrm{medium}} - v_{\mathrm{medium}}\right)\frac{k_z}{c^2} - \left(\varepsilon(\omega') - v_{\mathrm{medium}}^2/c^2\right)\frac{\omega}{c^2} - \frac{1}{2}\frac{\omega^2}{c^2}\left(1 + \frac{v_{\mathrm{medium}}}{v_{\mathrm{e}}}\right)^2\frac{\partial\varepsilon(\omega')}{\partial\omega}} \tag{S88}$$

$$v_{\mathrm{g},\rho} = \frac{-k_\rho\left(1 - v_{\mathrm{medium}}^2/c^2\right)}{\left(\varepsilon(\omega')v_{\mathrm{medium}} - v_{\mathrm{medium}}\right)\frac{k_z}{c^2} - \left(\varepsilon(\omega') - v_{\mathrm{medium}}^2/c^2\right)\frac{\omega}{c^2} - \frac{1}{2}\frac{\omega^2}{c^2}\left(1 + \frac{v_{\mathrm{medium}}}{v_{\mathrm{e}}}\right)^2\frac{\partial\varepsilon(\omega')}{\partial\omega}} \tag{S89}$$

where θ_{rCR} is the angle between the particle velocity $\bar{v}_{\mathrm{e}} = -\hat{z}v_{\mathrm{e}}$ and the group velocity $\bar{v}_{\mathrm{g}} = \hat{z}v_{\mathrm{g},z} + \hat{\rho}\bar{v}_{\mathrm{g},\rho}$ of the reversed Cherenkov radiation, and $\varepsilon(\omega') = n^2(\omega')$ is the dispersive and dissipative relative permittivity under the medium co-moving frame [42]. A close inspection of the expression of θ_{rCR} in equation (S87) shows two facts. First, there is no emergence of the frequency-dispersion related term $\partial\varepsilon(\omega')/\partial\omega$ in equation (S87), indicating the frequency dispersion of material would not change the direction of group velocity of the emitted reversed Cherenkov radiation. In fact, this frequency-dispersion related term only shows up in equation (S88-S89), indicating this term may modify the magnitude of group velocity to some extent. Second, the material loss manifests only via the real-part operator $\mathrm{Re}\{\cdot\}$ in equation (S87). Together, these two facts indicate that the reversed Cherenkov angles in dispersive and dissipated moving media are relatively consistent with those in nondispersive and lossless media, as shown in Figs. R4(a) and R4(b). Meanwhile, on the basis of equation (S87), the generalized form of the medium velocity threshold required for the emergence of reversed Cherenkov radiation in presence of reasonable frequency dispersion and material loss is obtained as

$$v_{\text{th,rCR,medium}} = \text{Re}\{c/\varepsilon(\omega')\} = \text{Re}\{c/n^2(\omega')\} \tag{S90}$$

According to equation (S90), we show in Fig. S6(a) that the reasonable material would have negligible influence on the medium velocity threshold $v_{\text{th,rCR,medium}}$. Above this threshold, we further show in Fig. S6(b) that the realistic material dispersion and loss would to some extent broaden the angular distribution of reversed Cherenkov radiation.

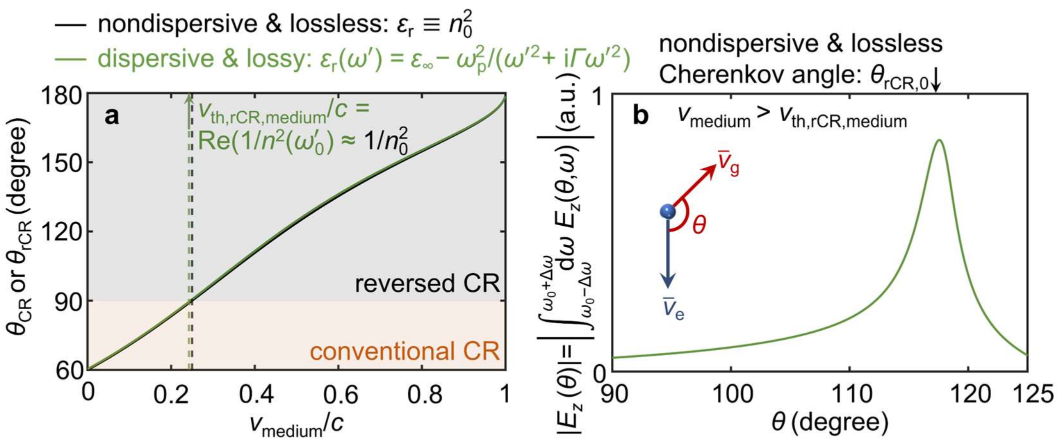

FIG. S6. Influence of the frequency dispersion and material loss on reversed Cherenkov radiation via Fizeau-Fresnel drag. Here $v_e/c = 0.9999$. For conceptual illustration, we set that the dispersive and dissipative medium has a relative permittivity of $\varepsilon_r(\omega') = n^2(\omega') = \varepsilon_\infty - \omega_p^2/(\omega'^2 + i\Gamma\omega')$, where $\varepsilon_\infty = 20$, $\omega_p/2\pi = 40$ THz, and $\Gamma/2\pi = 0.5$ THz. At the working frequency under the medium co-moving frame $\omega_0'/2\pi = \omega_0\gamma(1 + v_{\text{medium}}/v_e)/2\pi = 10$ THz, $n(\omega_0') = n_0 + i0.2 = 2 + i0.2$. (a) Dependence of the Cherenkov angle on the moving-medium velocity. (b) Angular field distribution $|E_z(\theta)| = |\partial E_z(r,t)/\partial\theta| = \left|\int_{\omega_0-\Delta\omega}^{\omega_0+\Delta\omega} d\omega\, E_z(\theta,\omega)\right|$ over a bandwidth $\Delta\omega/\omega_0 = 1\%$, where $v_{\text{medium}} = 0.45c > v_{\text{th,rCR,medium}}$. As shown in (a) and (b), the reversed Cherenkov angle and the medium velocity threshold remain qualitatively valid in presence of both the frequency dispersion and material loss.

S5.5 Connection to quantum friction

In this subsection, we briefly discuss the conceptual relations of our findings to quantum friction. Our revealed Cherenkov radiation is conceptually relevant to quantum friction in terms of the basic mechanism of motion-induced Fizeau-Fresnel drag and the widely-used isofrequency contour arguments for moving media. Yet, while the radiation in quantum friction typically originates from the thermal or quantum fluctuation, our revealed reversed Cherenkov radiation has a unique physical origin from the interactions of charged particles with moving media.

Reference

113. T. G. Philbin and U. Leonhardt, "No quantum friction between uniformly moving plates," New J. Phys. **11**, 033035 (2009).
114. J. B. Pendry, "Quantum friction–fact or fiction?," New J. Phys. **12**, 033028 (2010).
115. U. Leonhardt, "Comment on 'Quantum Friction—Fact or Fiction?'," New J. Phys. **12**, 068001 (2010).
116. J. B. Pendry, "Reply to comment on 'Quantum friction—fact or fiction?'," New J. Phys. **12**, 068002 (2010).
117. A. I. Volokitin and B. N. J. Persson, "Comment on 'No quantum friction between uniformly moving plates'," New J. Phys. **13**, 068001 (2011).
118. T. G. Philbin and U. Leonhardt, "Reply to comment on 'No quantum friction between uniformly moving plates'," New J. Phys. **13**, 068002 (2011).